ABSTRACT

Title of Document: DEVELOPMENT OF VIDEO IMAGE DETECTION ALGORITHM FOR SMOKE PLUMES

Alan J. Kouchinsky, Master of Science, Fire Protection Engineering, 2007

Directed By: Associate Professor and Associate Chair, James A. Milke, Department of Fire Protection Engineering

The objective of this work is to develop a predictive activation time algorithm for smoke plumes for axonX's SigniFire video image detection (VID) system from recent tests in a large volume space performed at the University of Maryland's (UMD) Cole Field House. The SigniFire system was able to detect a smoke plume from distances of 37.8 m (124 ft) to 54.9 m (180 ft) typically before the smoke reached the ceiling. The goal is to establish an understanding of the significant parameters affecting activation time based on observations and trends from the video image data. As a result of the understanding, insight into a predictive algorithm is developed, which is the first step toward future use of the VID system for a performance based design.

DETERMINATION OF SMOKE ALGORITM ACTIVATION FOR VIDEO IMAGE DETECTION

By

Alan J. Kouchinsky

Thesis submitted to the Faculty of the Graduate School of the
University of Maryland, College Park, in partial fulfillment
of the requirements for the degree of
Master of Science
2007

Advisory Committee:
James A. Milke, Chair
Frederick W. Mowrer
Peter B. Sunderland

Acknowledgments

I would like to acknowledge the Maryland Industrial Partnerships (MIPS) program in the Maryland Technology Enterprise Institute for supporting this research to help axonX further their understanding and performance of the SigniFire system. This project would not have been possible without the generosity of Curt Callahan allowing us to test at Cole Field House. The support of axonX was invaluable and a great appreciation is expressed to Andy Lynch for his guidance and expertise. Additionally, the helpfulness of Jacob Deutchman was essential for completing the testing within a short time period. A special thanks to my advisory committee of Dr. Milke, Dr. Mowrer, and Dr. Sunderland. Lastly, I would like to thank Dr. Milke for his dedication to education and his wisdom to help guide my thesis to its completion.

Table of Contents

Acknowledgments ii
Table of Contents iii
List of Tables iv
List of Figures v
Nomenclature vi
Acronyms Used vii
1 Introduction 1
2 Objective 2
3 Literature Survey 3
3.1 VID Technology 3
3.2 VID Systems and Performance 3
3.3 Plume Dynamics 13
4 Experimental Program 17
4.1 Experimental setup 17
4.2 Instrumentation 19
4.3 Fire Sources 25
4.4 Procedure 26
5 Data 27
5.1 Activation Times 27
5.2 Optical Density and Temperature Measurements 28
5.3 Photometric Survey 33
6 Development of Predictive Algorithm 36
6.1 Qualitative Review of Data 36
6.2 Parameters of Interest 39
6.3 Optical Density Calculation 41
6.4 Normalization of Time 46
6.5 Analysis 49
6.6 Results 55
7 Conclusion 63
8 Future Research 64
References 66

List of Tables

Table 1 - NRL Fire and Nuisance Sources 7
Table 2 - Distance to Source at Location A from Cameras 22
Table 3 - Cole Field House Fire Sources 25
Table 4 - Activation Time and Alarm for 4 min emitter at Low Lighting 27
Table 5 - Activation Time and Alarm for 8 min emitter at Low Lighting 27
Table 6 - Activation Time and Alarm for 4 min emitter at High Lighting 27
Table 7 - Photometric Measurements taken at Low Lighting 34
Table 8 - Photometric Measurements taken at High Lighting 34
Table 9 - Comparison of Activation Times for Different Lighting Levels for 4 min emitter 36
Table 10 - Calculated $\dot{V}$ from Mass Plume Entrainment Correlations for Heskestad 43
Table 11 - Fuel Parameter Estimation from Optical Density 45
Table 12 - Optical Density at Varying Height and Range of Fuel Parameter 46
Table 13 –Time to Enter FOV 47
Table 14 – Normalized Activation Time for 4 min emitter at Low Lighting 48
Table 15 – Normalized Activation Time for 8 min emitter at Low Lighting 48
Table 16 - Normalized Activation Time for 4 min emitter at High Lighting 48
Table 17 - Contrast Ratio for 4 min emitter at Low Lighting 51
Table 18 - Contrast Ratio for 8 min emitter at Low Lighting 52
Table 19 - Contrast Ratio for 4 min emitter at High Lighting 52
Table 20 - Plume Outline Growth Rate for 4 min emitter at Low Lighting 54
Table 21 - Plume Outline Growth Rate for 8 min emitter at Low Lighting 54
Table 22 - Plume Outline Growth Rate for 4 min emitter at High Lighting 55
Table 23 - Regression Analysis Statistical Output 57
Table 24 - Confidence of Regression Coefficients 58
Table 25 - ANOVA Statistical Output 59
Table 26 - Regression Analysis Statistical Output (Modified) 61
Table 27 - Confidence of Regression Coefficients (Modified) 61
Table 28 - ANOVA Statistical Output (Modified) 61

List of Figures

Figure 1 – Representative VID System Layout 5
Figure 2 - Overall Schematic of Cole Field House 18
Figure 3 - Lighting Orientation of Cole Field House 19
Figure 4 - Locations of Cameras and Sources in Cole Field House 20
Figure 5 - Images of All Eight Cameras for Cole Field House Tests 21
Figure 6 - Instrumentation Apparatus for Cole Field House 24
Figure 7 – ODM and Thermocouple Setup for Cole Field House 24
Figure 8 – Plume Tilt Depiction for 4 min Emitter at Low Lighting Level 28
Figure 9 - Optical Density at 1.19 m (4 min emitter at Low Lighting) 29
Figure 10 - Optical Density at 2.72 m (4 min emitter at Low Lighting) 29
Figure 11 - Optical Density at 1.19 m (8 min emitter at Low Lighting) 30
Figure 12 - Optical Density at 2.72 m (8 min emitter at Low Lighting) 30
Figure 13 - Optical Density at 1.19 m (4 min emitter at High Lighting) 30
Figure 14 - Optical Density at 2.72 m (4 min emitter at High Lighting) 31
Figure 15 - Thermocouple Temperatures (4 min emitter at Low Lighting) 32
Figure 16 - Thermocouple Temperatures (8 min emitter at Low Lighting) 32
Figure 17 - Thermocouple Temperatures (4 min emitter at High Lighting) 32
Figure 18 - Schematic of Photometric Survey Locations at Cole 33
Figure 19 – Graphical Depiction of Photometric Measurements 34
Figure 20 - Graphical Depiction of Photometric Measurements 35
Figure 21 - Lighting Level Effect on Activation Time 37
Figure 22 - Comparison of Activation Times at Low Lighting Level 38
Figure 23 - Comparison of Activation Times at High Lighting Level 39
Figure 24 - Contrast Effect on Algorithm Activation 41
Figure 25 - Images used to Determine Contrast Ratio 51
Figure 26 - Contrast Ratio for Three Tests and Eight Cameras 52
Figure 27 - Pixel Count Process Before and After 53
Figure 28 - Regression Analysis of Experimental versus 56
Figure 29 - Regression Analysis of Experimental versus 60

Nomenclature

C	contrast between plume and background
c_p	specific heat of plume gases, kJ/kg-K (Btu/lbmºF)
D	distance to source from camera (m)
δ	optical density per unit distance, m^{-1} (ft^{-1})
δ_m	mass optical density, m^2/g (ft^2/lb)
g	acceleration of gravity, m/s^2 (ft/s^2)
G	plume outline growth rate ($s-^1$)
H	height above fuel source, m (ft)
ΔH_f	net heat of combustion, kJ/kg (Btu/lb)
I	light intensity (lux)
L_e	lesser luminance
L_g	greater luminance
$\dot{m}_f$	mass loss rate of fuel burned, kg/s (lb/s)
$\dot{m}_{pl}$	mass flow in plume at height z, kg/s (lb/s)
ρ_∞	density of ambient air, kg/m^3 (lb/ft^3)
ρ_{pl}	density of plume gases, kg/m^3 (lb/ft^3)
$\dot{Q}$	heat release rate of fire, kW (Btu/s)
$\dot{Q}_c$	convective heat release rate of fire, kW (Btu/s)
T_c	absolute centerline axisymmetric plume temperature at elevation z, K (R)
T_∞	absolute ambient temperature, K (R)
t_{pl}	transport time lag of plume, s (s)
$\dot{V}_{pl}$	volumetric smoke flow at elevation z, m^3/s (cfm)
χ_a	combustion efficiency
z	height above fuel, m (ft)
z_0	virtual origin correction of the axisymmetric plume, m (ft)

Acronyms Used

ADC	Advanced Damage Countermeasures
ANOVA	Analysis Of Variance
AOI	Area of Interest
CCTV	Closed Circuit Televisions
EST	Edwards System Technology
FOV	Field of View
HRR	Heat Release Rate
HSD	Heat Sensing Device
HTA	High Temperature Alarm
MFRI	Maryland Fire & Rescue Institute
MIPS	Maryland Industrial Partnership System
NFPA	National Fire Protection Association
NRCC	National Research Council of Canada
NRL	Naval Research Laboratory
ODM	Optical Density Meter
SFA	Smoke and Fire Alert
SIFSS	Shipboard Intelligent Fire Suppression System
UL	Underwriters Laboratory
UMD	University of Maryland
VID	Video Image Detection
VSD-8	Visual Smoke Detection
VSP	Volume Sensor Prototype

1 Introduction

A spot detector relies on the products of combustion (particulates, gases, and heat) from a fire to diffuse to a given detector for activation. Circumstances arise when conventional smoke and fire detectors do not activate in a timely manner due to the height and temperature profiles within the space. Video-based smoke and fire detection enables a space to be monitored remotely by optical detection technology that relies on spectral information and not effluents from a combustion source reaching a particular detector location [1].

The development of better computer processing and imaging analysis technologies has given rise to the ability to use a standard Closed Circuit Television (CCTV) camera for more than a standard video surveillance and monitoring system. The ability to use existing surveillance equipment for real time fire detection has prompted research to further understand the applications and feasibility of such a VID system for many applications including tunnels, power plants, large volume spaces, and naval ships [1].

2 Objective

The objective of this study is to predict the activation time for a smoke plume algorithm for axonX's video-based fire detection system from experimental results performed in a large volume space, Cole Field House, at UMD. The focus of this thesis is to identify and quantify the role of major parameters affecting detection time with the intent to provide an alternate algorithm that can be used to improve an existing algorithm. This analysis is independent of any knowledge of the functionality of the underlying algorithm and is based instead on imaging analysis and fundamentals of fire dynamics. Additionally, this thesis is a first step toward developing a predictive algorithm for the use of a VID system in a performance based design.

3 Literature Survey

3.1 VID Technology

A VID system evaluates live video through algorithms that focus on the identification of any change that indicates the onset of fire conditions. These algorithms may examine many different characteristics of an image such as contrast, color, brightness variations, and movement to discriminate fire conditions from every day activities.

A VID system can be classified as a machine vision. This concept is basically the replacement of human involvement (inspection and monitoring) of a space by "utilizing video or photographic images with computer processing schemes to extract desired information. Once an image is obtained and digitized for computer input, the image is processed to extract key features and then these features are analyzed for specific information" [1]. This technology is used in industries typically for monitoring production and quality control [1].

The application of this technology for fire detection is more challenging. For this application, the process is designed to look at abnormalities of fire conditions from these associated with normal operations of everyday activity such as people movement, equipment operation, and ambient conditions [1].

3.2 VID Systems and Performance

Three major companies have developed video-based fire detection systems. All three commercial systems are applications of machine vision technology that use live video images along with proprietary algorithms to detect the onset of fires. AxonX

(Maryland) has developed the SigniFire system, selected for this study. The SigniFire system uses up to 8 CCTV cameras and software-based algorithms that run on PC platforms. The system has the ability to detect smoke through an ambient (onset of smoke layer) and plume pattern recognition algorithm. SigniFire can also detect a flaming fire within a 6 by 6 pixel area of the image if the flame is within the camera's line of sight. Lastly, the system is able to detect a fire by means of a reflective algorithm that looks at the reflected fire light from walls or other objects when the fire is not in the line of sight of a camera [2].

Fastcom Technology (Switzerland) along with a recent partner acquisition, Securiton, has developed Smoke and Fire Alert (SFA). The SFA system uses up to 16 CCTV cameras and software-based algorithms that run on PC platforms. The algorithms use the latest image processing technology by examining several parameters such as contrast, color, movement, and outline. The system functions by assessing the fire situation through a set of independent algorithms that run in parallel while a decision algorithm monitors their individual contributions in real-time. The system can detect flaming and smoldering fires through a fire and smoke algorithm [3].

Fire Sentry Corporation (California) has created Visual Smoke Detection (VSD-8). The VSD-8 system uses up to 8 CCTV cameras linked to a self-contained processing system. Smoke is detected by looking for small areas of change within the video image at the digitization stage. The images showing change are filtered further looking for characteristics of smoke. The VSD-8 system only has the ability to detect smoke and not flames. For a wider array of applications, the system can adjust the parameters such as

quantity of smoke and the duration of time that smoke is present before an alarm is activated [4].

Upon activation of an algorithm, the notification of the event is similar to that of a spot-detector system. However, the VID system is able to give visual notification to a surveillance operator or Fire Department. Figure 1 is a depiction of axonX's system as a representative setup of the system architecture of all three systems [2]. Typically, up to eight CCTV security cameras are connected to a computer processor where the image is analyzed with each company's proprietary algorithms. The images are transferred to an operator's console for monitoring. When an alarm is activated, the image is archived and the alarm is shown on the operator's console. The alarm can be sent to a remote monitoring service for an assessment of fire fighting capabilities needed and imminent threat or danger.

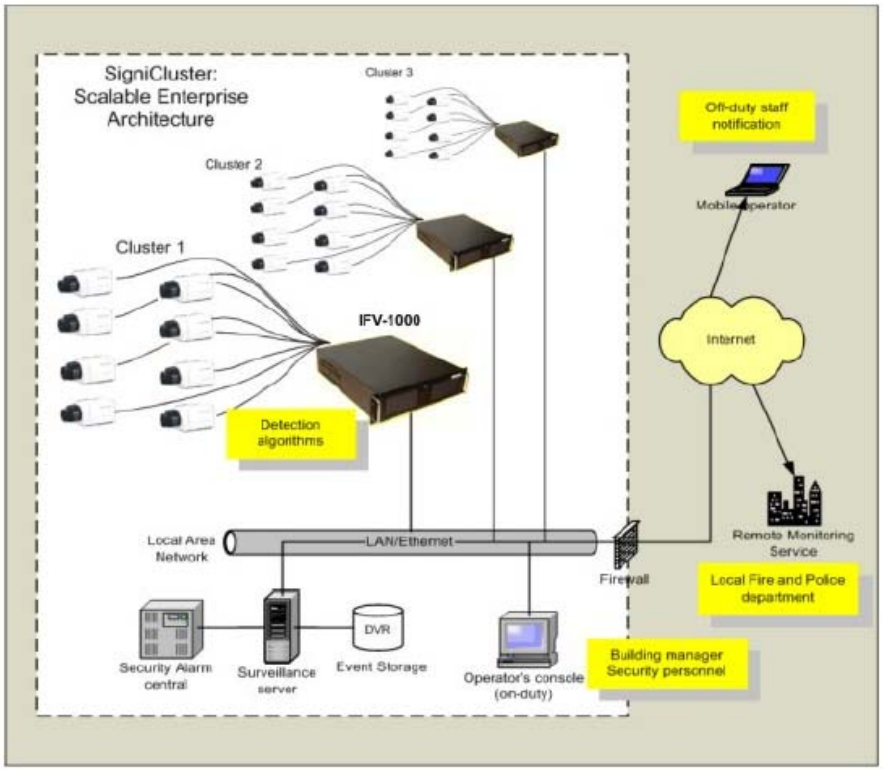

Figure 1 – Representative VID System Layout

The three video-based fire detection companies described above were chosen to be evaluated by the Naval Research Laboratory (NRL) as part of a detection research project for the United States Navy. The Advanced Volume Sensor Task was created under the US Office of Naval Research, Future Naval Capabilities program, Advanced Damage Countermeasures (ADC), to develop a detection system that could identify shipboard control conditions over a five year program [1]. The Navy's objective of such a detection system was to provide an alarm for events such as flaming and smoldering fires, explosions, pipe ruptures, and flooding on shipboard applications. The volume sensor concept was intended to use existing surveillance cameras with the intent of having the ability to provide multiple system functions with minimal modifications to the infrastructure of the naval ship. Additionally, the desired volume sensor should have the ability to detect a fire throughout an entire space without relying on a conventional spot detector.[1] The focus of a multi-criteria detection approach was to increase the sensitivity of the system to real fires and to reduce the susceptibility to nuisance alarm sources [1, 5].

The NRL research effort was divided into five phases. The first phase of research in the NRL program consisted of a review of current and emerging technologies for video, optical, and acoustic methods with the intent to identify the most plausible system to meet the program objectives. The conclusion of the initial evaluation was that the program would investigate alternative sensing methods through two parallel efforts. The first effort would use "pattern recognition methods of video camera images (machine vision: spatially resolved) and the other emphasizing resolved detection methods. The volume detection capability will be achieved by combining point sensors with optical

[1] The Navy reports referred to the spot-type detectors as "point-type" detectors.

detectors (machine vision), OFD and/or beam smoke detectors (and possible others such as acoustic) with signal processing achieved using a neural network" [1].

The second phase of NRL research consisted of the first round of full-scale testing that was performed on two VID systems, SFA and VSD-8. The performance characteristics of the VID systems were compared to those of addressable spot-type ionization and photoelectric smoke detectors to assess the future applicability of the VID system for shipboard use. The tests were performed in a laboratory that consisted of a 10 m x 10 m x 3 m (33 x 33 x 10 ft) compartment that was cluttered with multiple structures to provide visual obstructions. The test series used a total of 14 fire and smoldering sources and 11 nuisance sources at 7 test locations as listed in Table 1.

Table 1 - NRL Fire and Nuisance Sources

Smoldering	Flaming	Nuisance
Bag of trash	Lactose/chlorate	Cigarette smoke
Cable bundle	Trash can	Aerosol deodorant
Wire	Mattress and bedding	Toaster: overdone toast
Printed circuit board	Heptane pan	Welding
Laundry	JP-5 pan	Torch cut painted steel
Mattress and bedding	Cardboard box	Grinding unpainted steel
Computer Monitor		Cutting unpainted steel
Smoke pellets		People working on ladders
		Waving a towel
		Turning lights on and off
		Sunlight

*The fire sources are classified by their initial burning characteristics.

The test results indicated that the VID systems "using only smoke alarm algorithms can provide faster detection than point-type smoke detectors" [6]. One exception to the overall faster performance was that the VID systems "did not respond to small flaming fires as well as ionization smoke detectors" [6]. Additionally, the VID

systems "demonstrated comparable nuisance alarm immunity to the point-type smoke detection systems" [6], but alarmed inappropriately to people moving in the space.

The third phase of NRL research consisted of a continuation of the evaluation of the VID system onboard the ex-USS Shadwell, the Naval Research Laboratory full-scale research facility in Mobile, Alabama. The first test series was Test Series 2 of the CVN 21 Fire Threat to Ordnance program conducted April 7-18, 2003. The testing environment represented magazine storage onboard CVNX class ships to further test the VID deficiency in detecting flaming fires quickly [7]. During these tests, the VID systems were evaluated in an environment designed to represent storage onboard ships while exposed to two fire scenarios: adjacent space and interior fires. Similarly to the last test series, two VID systems were tested, SFA and VSD-8. The VID systems were compared to commercial ionization, photoelectric and heat detectors as well as an existing Navy magazine detection system, which was comprised of heat sensing devices (HSDs) and high temperature alarms (HTAs). The tests were performed in a small magazine area (2nd deck) with dimensions of 6.05 m x 3.61 m x 3.05 m (19.83 ft 11.83 ft x 10 ft) and a medium magazine area (3rd deck) that was 5.94 m x 8.08 m x 3.05 m (19.5 ft 26.5 ft x 10 ft). The spaces contained visual obstructions representative of ordnance stowage conditions which included a variety of different sized metal cabinets. The test series used two fires sources, heptane spray in the adjacent space and different sizes of wood crib fires, with heat release rates ranging from 25 to 250 kW (23.7 to 237 Btu/s) in the magazine space. The SFA system detected most of the wood crib and heptane fires on the 2nd deck, but only detected two of the wood crib fires on the 3rd deck. The VSD-8 performed poorly, as it did not alarm in any fire test. The manufacturer of the VSD-8

system reported that the "camera iris settings were open too wide causing a decrease in contrast that prevented proper detection" [8]. From the literature, it is not clear which of the algorithms for the SFA system were evaluated in this test series.

Due to the limited fire scenarios that were conducted during the CVN21 Test Series 2, an additional test series was conducted specifically for the Volume Sensor program to provide a broader range of fire and nuisance sources exposures. This second test series, Series VS1 was also conducted on the ex-USS Shadwell from April 21-25, 2003. The tests were performed in the same spaces as tested in the CVN21 Test Series 2. The test series used three of the sources from the phase 2 test noted in Table 1 [6]. The three fires sources used in the second test series were: cable bundle, lactose/chrolate, and a cardboard box at 6 locations on each deck. An additional 6 nuisance sources were tested, including torch cut steel, grinding a painted bulkhead, cutting steel, people working in the space, waving material, and welding. Three VID systems were tested in this series: SFA, VSD-8, and SigniFire. The SFA utilized both flame and smoke algorithms, VSD-8 used only a smoke algorithm, and SigniFire utilized a flame and smoke algorithm for detection. The VID systems were compared against the same commercial and Navy detectors except for the HTAs as was tested in CVN21 Test Series 2. The test results showed that the SigniFire system "clearly performed better than the SFA and VSD-8 systems." The system detected "all of the flaming fires, 16 of 20 smoldering fires and only false alarmed for 2 nuisance sources (both of which were welding events)" [9]. Consistent with the previous test series, the VSD-8 system performed poorly, only alarming to two fire tests. Once again, the manufacturer reported that the disappointing performance was due to the settings of the camera iris. The SFA

system “did not perform as well as the smoke detection systems regarding the total number of correct classification” [9] but when it did alarm, “the SFA system was generally faster than the spot-type smoke detectors to alarm to smoldering fires and was generally comparable in speed for flaming fires” [9].

The next test series (VS2) expanded on the VS1 test series with respect to the size and orientation of the compartments used. The tests were conducted in a laboratory that consisted of a 10 m x 10 m x 3 m (33 x 33 x 10 ft) compartment that was divided into three compartments and a passageway that were of similar size to the spaces on the ex-USS Shadwell. The compartments contained multiple visual obstructions such as electrical cabinets, chairs, tables, office equipment, cable trays and ductwork. The test series evaluated SFA, VSD-8, and SigniFire to 12 flaming and smoldering fire sources and 11 nuisance sources at 11 testing locations. The fire and potential nuisance sources were almost identical to the 2nd phase of testing [6]. Two additional fire sources were added: flaming cardboard box filled with plastic and a smoldering trash can. The sources not used from this test series were smoke pellets, lactose/chlorate, heptane pan, and JP-5 pan. Similarly, the additional nuisance sources included a person working in the compartment, people working in the compartment, flashlight, flashbulb and removed torch cut painted steel, people working on ladders, & turning lights on and off. In addition, various lighting conditions in the space were tested such as general, red, yellow, low level white, emergency and darkened ship illumination. Another parameter of interest tested was the two different background colors in the space. The SFA system utilized both flame and smoke algorithms, the VSD-8 system used only a smoke alarm

algorithm, and the SigniFire system used a fire, smoke, and reflective (detect fires outside the field of view (FOV)) algorithm [10].

Similar to past tests, the VID systems were compared to addressable spot-type ionization and photoelectric smoke detectors as a benchmark for performance. The test results indicated that the commercial VID technologies alarmed to more sources faster than the spot-type detection systems during the series of 83 multiple source fire tests. In particular, the SFA and SigniFire VID systems were the only systems capable of detecting 95% of the fires or better [10]. The next best system was the Edwards System Technology (EST) ionization detection system which detected 81% of the fires. The VSD-8 system detected only 63% of fires and was comparable to the other commercial ionization and photoelectric detectors (59% - 64%) [10].

The fourth and fifth phase of research of the NRL test series was done to evaluate the Volume Sensor Prototype (VSP) that used both VID technology along with spectral and acoustic sensors which was then processed by a fusion machine (data fusion of algorithms). The tests performed included the results of the VSPs, VID systems, and commercial detectors. The tests were consistent with the overall orientation, flaming and smoldering fire sources as well as nuisance sources from the previous tests discussed. Additional results can be found in references [11 – 13].

Outside of the comprehensive testing completed by the NRL on the three commercial VID technologies, additional testing has been completed on each VID system to broaden the applicable markets. AxonX has tested the SigniFire system for many applications. One of the most recent tests was performed at the University of Maryland. The tests series was designed to test the performance of the system for a multi-room

structure similar to that of a dormitory style orientation performed at Maryland Fire & Rescue Institute (MFRI). The test series used a total of 9 fire and smoldering sources and 5 nuisance sources at 3 test locations in the room of origin. The results indicated that the SigniFire system performed significantly better than the traditional smoke and fire detection systems on average for every fire test [14]. The system detected 100% of all fire sources in the room of origin and 85% in the adjacent hallway. The ionization and photoelectric detectors detected 74% and 78% of all fire sources in the room of origin and 67% and 70% in the adjacent hallway, respectively [14].

One of the more intriguing test programs was the use of SigniFire as the means of detection for a Shipboard Intelligent Fire Suppression System (SIFSS) for the Royal Navy [15]. The research focused on the ability to automatically locate and correctly size the fire and then instruct a robotically aimed low consequence suppression system to suppress the fire. A combination of two parallel cameras at a given level along with a similar orientation in the vertical direction gave the ability to triangulate the fire location in a three dimensional space. Additionally, the heat release rate of the flaming fire was estimated.

Testing has also been performed on warehouse scenarios at Aberdeen Proving Ground (Maryland) that involved liquid pan fires at distances on the order of 30 m (100 ft). Testing also included the potential for nuisance alarms such as strobe lights. Future testing plans at Aberdeen during July 2007 will focus on the performance in an outdoor environment [16].

The National Fire Protection Association (NFPA) Research Foundation has partnered with axonX to test the system in the Lincoln Tunnel (New York) for everyday

nuisance alarms. Similarly, the National Research Council of Canada (NRCC) has tested the system in a tunnel environment with liquid pan fires. Several physical setups were tested that involved cars and walls blocking the fire. Future testing plans within the Montreal Tunnel (Canada) are planned for the fall of 2007 with the intent to use smoke emitters as the fire source similar to the testing at UMD [16].

SFA has been targeted toward applications that include motorway tunnels, outdoor areas (car parks, industrial sites, etc.) and large indoor facilities (power plants, warehouses, etc) [3]. The company has tested the system in a tunnel and was briefly presented at the Twelfth International Conference on Automatic Fire Detection and another has been operating for one and half years in a large space of a nuclear facility [1]. VSD-8 claims that systems are installed throughout various applications including electrical power generating stations (nuclear, fossil & wood), industrial sites, aircraft hangers, road and rail tunnels [4]. However outside of the NRL test series, no results from these additional experimental programs about the performance of the SFA and VSD-8 systems are known.

3.3 Plume Dynamics

One of the characteristics of VID systems is the ability to detect smoke plumes. The recent testing at Cole Field House focused on the detection of an axisymmetric, point source plume. A plume is formed when a mass of hot gases from a fire is surrounded by colder gases (ambient air). The hotter and less dense mass will rise upward due to the density difference between the hot gases and ambient air. The buoyant flow results in a smoke plume that has several distinct properties. The experimental research of Heskestad has defined the underlying principles and attributes of smoke plumes.

The highest temperature and velocity of the plume is along the centerline and tends to decrease across the plume radius to the edge of the plume following a Gaussian profile. The centerline temperature and velocity are known to decrease with height due to the effect of increasing air entrainment of cool air [17]. Heskestad [18] developed a centerline plume temperature correlation as shown in Equations (1) - (2).

The properties listed below were used for the variables throughout the equations for normal properties of air:

T_∞ = 293K (68ºF)
ρ_∞ = 1.2 kg/m^3 (0.0749 lb/ft^3)
g = 9.81 m/s^2 (32.17 ft^2/s)
c_p = 1.0 kJ/kg-K (0.240 Btu/lbmºF)
$\dot{Q}_c = 0.7\dot{Q}$

Heskestad's plume temperature correlation is presented as Equation 1. The virtual origion (z_o) is a method proposed by Heskestad to account for "area sources", i.e., fires that account for large areas.

.

$$T_c = 9.1\left(\frac{T_\infty}{g c_p^2 \rho_\infty^2}\right)^{1/3} \dot{Q}_c^{2/3} (z - z_0)^{-5/3} + T_\infty \qquad (1)$$

The original equation can be simplified as follows with normal properties of air:

$$T_c = 25\dot{Q}_c^{2/3} (z - z_0)^{-5/3} + T_\infty \qquad (2)$$

Mowrer [19] was able to determine a lag time associated with smoke plumes based on the local velocity at a height above the source from Heskestad. A correlation for the transport time lag within the plume region is presented as Equation 3.

$$t_{pl} = 0.67\left(\frac{H^{4/3}}{\dot{Q}^{1/3}}\right) \tag{3}$$

The plume mass entrainment rate is defined as the total mass flowing upward at a certain height above the fuel source. Heskestad states that "the mass flow at a particular elevation in a fire plume is almost completely attributable to air entrained by the plume at lower elevations. The mass flow contribute by the fire source itself is insignificant in comparison" [17]. Heskestad [18] determined a plume mass entrainment rate correlation as shown by Equation 4.

Heskestad's correlation is presented as Equation 4 for the plume mass entrainment rate and applies at heights above the mean flame height (z > L).

$$\dot{m}_{pl} = 0.071\dot{Q}_c^{1/3}(z - z_0)^{5/3} - 0.00192\dot{Q}_c \tag{4}$$

A simple correlation relating the plume volumetric flow rate can be calculated from the plume mass entrainment rate by Equation 5 [20].

$$\dot{V}_{pl} = \frac{\dot{m}_{pl}}{\rho_{pl}} \tag{5}$$

In addition to temperature and velocity profiles in a smoke plume, the optical density follows a similar trend such that the optical density decreases with height due to the effect of increasing air entrainment of cool air. Optical density is defined as the transmittance of a light beam that can pass through visible smoke [20]. In addition, the optical density is directly related to the fuel properties of the burning object as shown by Equation 6 [21].

$$\delta = \frac{\delta_m \dot{m}_f}{\dot{V}_{pl}} = \left(\frac{\delta_m}{\chi_a \Delta H_f} \right) \left(\frac{\dot{Q}}{\dot{V}_{pl}} \right) \tag{6}$$

4 Experimental Program

4.1 Experimental setup

Large scale testing of the VID system was completed at Cole Field House at the campus of the University of Maryland on January 27-28, 2007. The weather condition for the 27th was a dry and clear day of 14ºC (58ºF) and -8ºC (18ºF) for the high and low temperature respectively. The 28th had temperatures of 5ºC (41ºF) and -2ºC (29ºF) for the high and low respectively with flurries in the afternoon. Cole Field House was the basketball arena for UMD's basketball teams from 1955 to 2002. Cole contains offices, classrooms, locker rooms, and an arena with a seating capacity of 14,596 as shown in Figure 2. The arena floor is 62 m x 34 m (205 ft x 110 ft) and has a height of 30 m (100 ft) at the apex of the ceiling. In addition, the concourse level measures 110 m x 76 m (360 ft by 250 ft) and is approximately 12 m (40 ft) above the floor level.

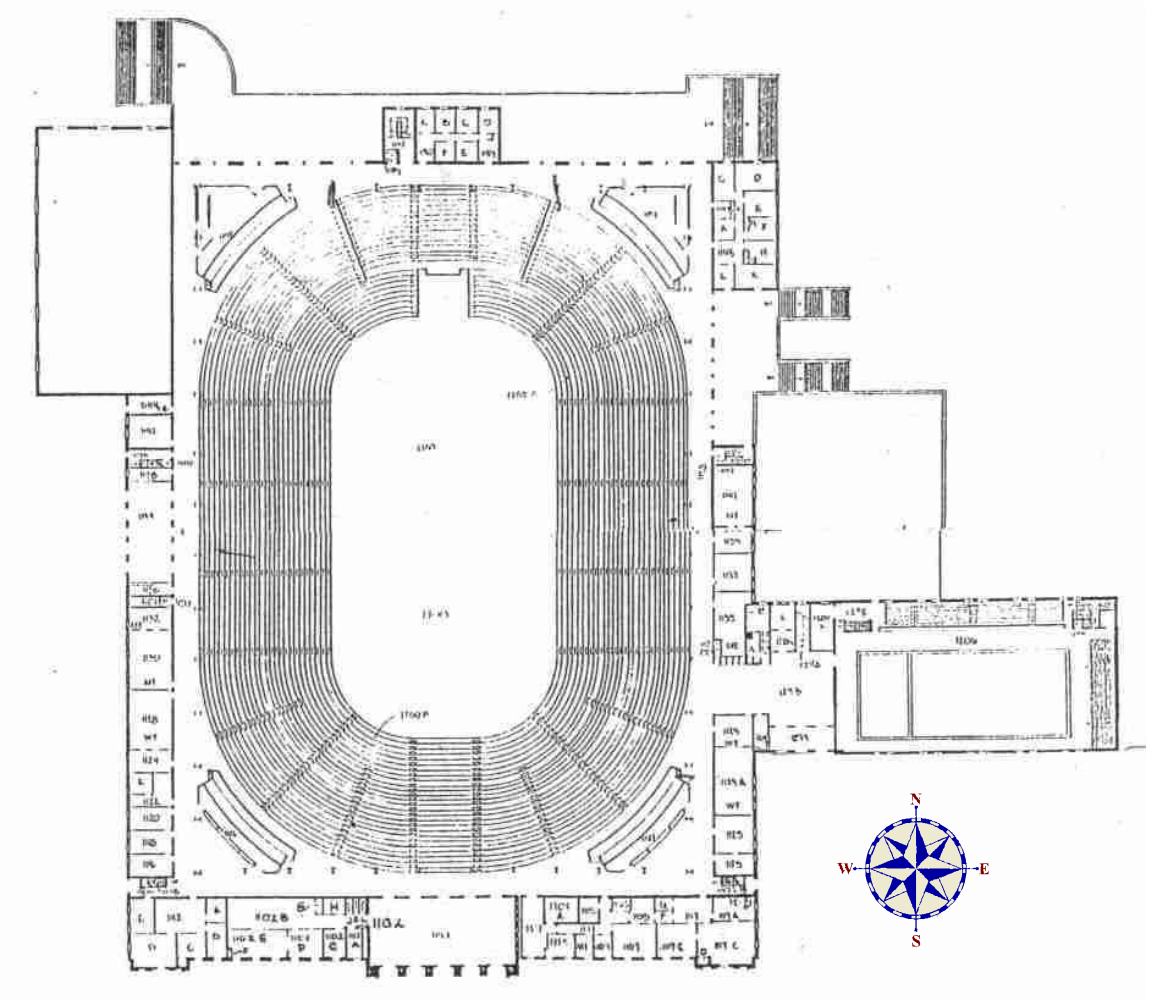

Figure 2 - Overall Schematic of Cole Field House

Cole Field House is constructed of masonry with a supporting steel frame structure. The ceiling above the concourse level has a flat dropped ceiling with acoustic tiles, such are typically found in business occupancies. The ceiling above the arena floor is a gradually increasing curved roof that has an apex at the middle of the arena floor. The arena floor has no visual obstructions to block the smoke view.

Lighting in the seating area is provided by metal halide lights near ceiling level. Each side of the arena (long side) consisted of three sets of light clusters. The lighting

consisted of a larger cluster at midpoint, and two additional at the far and near end of the arena floor as shown by Figure 3.

Figure 3 - Lighting Orientation of Cole Field House

A photometric survey was taken at ground level at the arena floor. Two lighting levels were used for testing: (1) low lighting level was 205.6 ± 105.5 lux (19.1 ± 9.8 foot-candles), (2) high lighting level was 712.6 ± 122.7 lux (66.2 ± 11.4 foot-candles). The low lighting level consisted of only the light cluster at the midpoint and the high lighting level consisted of the midpoint cluster and both the far and near end of the arena. The lighting level varied moderately over the arena floor due to direct light impingement at the point of measurement. The locations of the photometric survey readings are shown in section 5.3.

4.2 Instrumentation

The concourse level was instrumented with the eight CCTV cameras spaced symmetrically around the perimeter of the oval shaped seating area as shown in Figure 4.

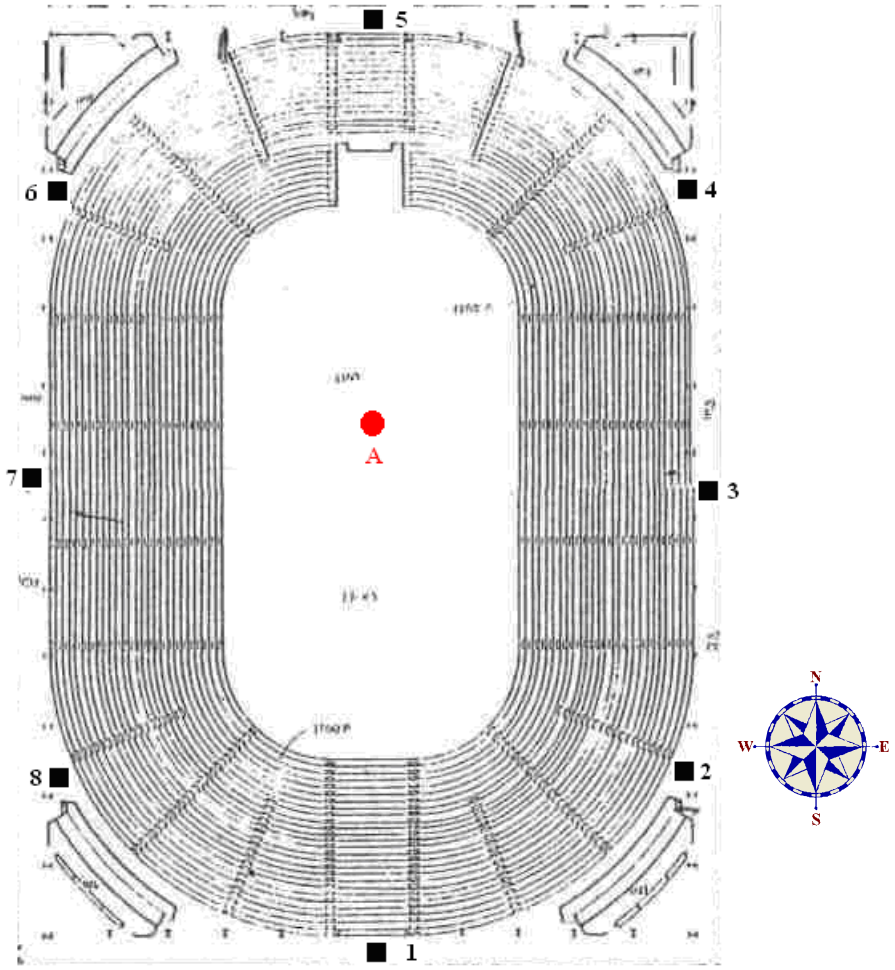

Figure 4 - Locations of Cameras and Sources in Cole Field House

Each camera was attached to a tripod and aligned horizontally. The cameras were directed at location A, 3 m (10 ft) north of the middle point of the arena floor. Figure 5 displays the images seen by each camera. Each image records the camera number in the lower left corner. The cameras are shown in numerical order left to right starting with camera 1 in the top left corner.

Figure 5 - Images of All Eight Cameras for Cole Field House Tests

The distance from each camera to the source ranged from 37.8 m to 54.9 m (124 ft to 180 ft). Table 2 lists the distance from each camera to the source at location A. The distance recorded only considers the distance in the horizontal direction to the source. In addition, the table gives an aspect of the overall FOV at the source location for each camera and the respective FOV angle which was determined from the original blueprint and images.

Table 2 - Distance to Source at Location A from Cameras

		Overall FOV of Image		
Camera	Distance (m)	Width (m)	Height (m)	FOV angle (°)
1	54.9	26.6	19.9	27.2
2	50.6	25	18.7	27.7
3	37.8	21.3	16	31.5
4	45.7	23.3	17.5	28.6
5	48.8	24.2	18.1	27.9
6	46	22.9	17.2	28.0
7	37.8	22.5	16.9	33.3
8	50.6	31.3	23.5	34.4

*Conversion: 1 m = 3.281 ft

All eight cameras were made by the same manufacturer, Bosch, model: 0335/20 with a fujinon lens. The cameras had an adjustable zoom which allowed the FOV to be changed. In addition, the lens had an automatic iris to adjust for dramatic lighting level changes typically associated with flaming fires. The image had a total of 76,800 pixels (320 x 240). The VID system was installed by a company representative to manufacturer specifications. The image was recorded by each camera and processed in real time by the VID processor. The signal from each camera was split four ways to process different sensitivities for each source, however only the default sensitivity (typical to most applications) was analyzed. The most recent version of the SigniFire algorithms on the date of testing was used.

In addition to the VID system that was present, measurements were taken for optical density and temperature in the plume at location A, as shown by Figure 6. The optical density measurements were taken at 1.19 m (3.90 ft) and 2.72 m (8.92 ft) above the source and the beam length spanned 1.5 m (5.0 ft). The optical density meters (ODM) were installed via recommendations from UL268 [22]. Additionally, five type K thermocouples were placed on the instrumentation apparatus at 0.3 m (1 ft) intervals at the centerline above the fire source starting at 1.42 m (4.66 ft) and up to 2.64 m (8.66 ft). Both the optical density and temperature measurements were recorded by a data acquisition system (NETDAQ) at 1 second intervals.

Six tank top radiant heaters (3 variable heat settings) from Dyno-Glo, model: RMC-TT15S were attached to propane tanks to provide a modest amount of thermal buoyancy to the smoke. The radiant heaters were set at the high heat setting of 4.40 kW (4.17 Btu/s) and placed within 60 cm (2 ft) around the source. The total heat output from the radiant heaters is equivalent to 26.4 kW. The middle of the radiant heater was at height of 25 cm (10 in.) above the fire source. A photograph of the arrangement of the heaters and instrumentation apparatus is presented as Figure 6.

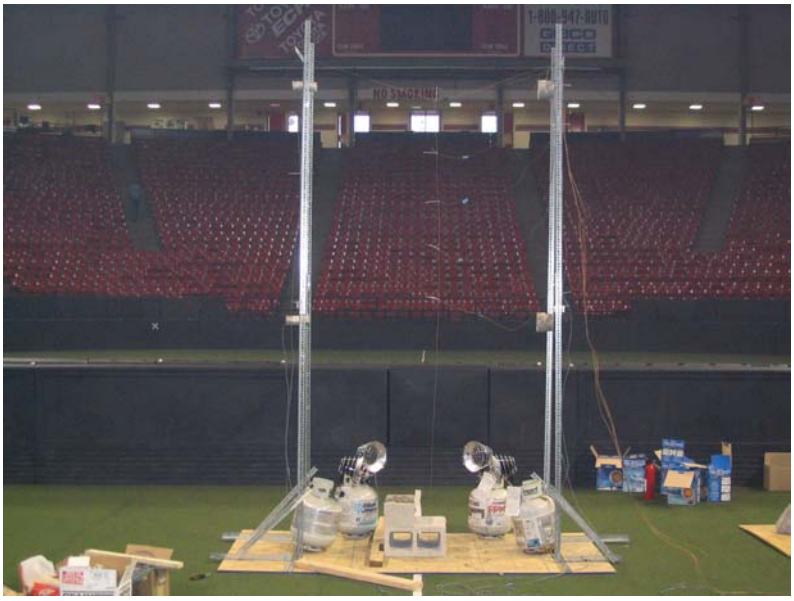

Figure 6 - Instrumentation Apparatus for Cole Field House

A close up picture of the placement of the ODMs and thermocouples on the instrumentation apparatus is presented as Figure 7.

Figure 7 – ODM and Thermocouple Setup for Cole Field House

4.3 Fire Sources

The VID system at Cole Field House was evaluated through a range of three tests using solely smoke emitters, with the smoke heated by the radiant heaters. The use of flaming sources was not permitted in the field house. All sources were used to test only the smoke plume algorithm of the VID system. All three sources were placed at location A (see Figure 4). The combinations of the fire sources and lighting conditions analyzed in this thesis are listed in Table 3.

Table 3 - Cole Field House Fire Sources

Location	Low Lighting Level Hot Emitter	High Lighting Level Hot Emitter
A	4 min	4 min
	8 min	-

All fire sources were placed on top of two cinder blocks at a height of 33 cm (13 in.) above floor level and ignited with a butane lighter. Both the 4 minute, model: S105 and 8 minute, model: S107 smoke emitters were products of Regin. The smoke production rate emitted was observed qualitatively to follow a constant output over the specified time duration. The 4 minute and 8 minute emitter had an initial mass of 60 grams (2.1 oz.) and 430 grams (15.2 oz.) respectively [23]. A whitish-gray color of smoke was emitted and became sufficiently buoyant due to the heat output created by the radiant heaters to reach the ceiling. It is noteworthy that the 8 minute emitter stopped producing smoke at 17 seconds into the test and then restarted at 30 seconds. This delay had an effect on the activation time for cameras 4 and 6, though all other cameras activated from the initial smoke plume during the first interval of smoke production. It is

interesting to note that cameras 4 and 6 produced images in which the smoke plume was the most significantly off center as shown by Figure 5.

4.4 Procedure

Prior to each test, the air was ventilated to ensure that the VID system was reset on a clean background. A two minute baseline condition was taken prior to the ignition of sources for a comparative measure for items such as the optical density. Once a source was ignited, the testing continued until all algorithms activated or after conditions were deemed to have reached steady state or self-extinguished, i.e., no additional detection alarms were anticipated.

5 Data

5.1 Activation Times

The detection times recorded from axonX's algorithm are presented in Table 4 through Table 6 for all eight cameras and sources conducted at Cole Field House.

Table 4 - Activation Time and Alarm for 4 min emitter at Low Lighting

	4 min (Low Lighting level)	
Camera	Alarm	$t_{activation}$ (s)
1	Smoke	27
2	Smoke	18
3	Smoke	31
4	Smoke	25
5	Smoke	40
6	Smoke	15
7	Smoke	23
8	Smoke	19

Table 5 - Activation Time and Alarm for 8 min emitter at Low Lighting

	8 min (Low Lighting level)	
Camera	Alarm	$t_{activation}$ (s)
1	Smoke	16
2	Smoke	15
3	Smoke	17
4	Smoke	148
5	Smoke	15
6	Smoke	41
7	Smoke	13
8	Smoke	16

*The smoke emitter stops production smoke at 17 seconds and restarts at 30 seconds

Table 6 - Activation Time and Alarm for 4 min emitter at High Lighting

	4 min (High Lighting level)	
Camera	Alarm	$t_{activation}$ (s)
1	Smoke	28
2	Smoke	24
3	Smoke	21
4	Smoke	40
5	Smoke	35
6	Smoke	80
7	Smoke	30
8	Smoke	25

5.2 Optical Density and Temperature Measurements

The optical density measurement for each test is displayed in Figure 9 through Figure 14. The optical density measurements on the whole were not accurate due to the air currents which slightly moved the smoke out of the beam of light. Figure 8 shows how the smoke was slightly tilted as it ascended through the ODM light beam and plume centerline thermocouple tree.

Figure 8 – Plume Tilt Depiction for 4 min Emitter at Low Lighting Level

Better optical density was taken for the 4 minute test under the high lighting level. Figure 13 and Figure 14 show how the obscuration within the light beam was relatively

constant for the duration of the test. Both the 4 and 8 minutes tests under the low lighting level did not provide great optical density results. Rather, the tests show a large degree of fluctuation and inconsistency throughout the test duration due to the air currents as shown by the ODM measurements.

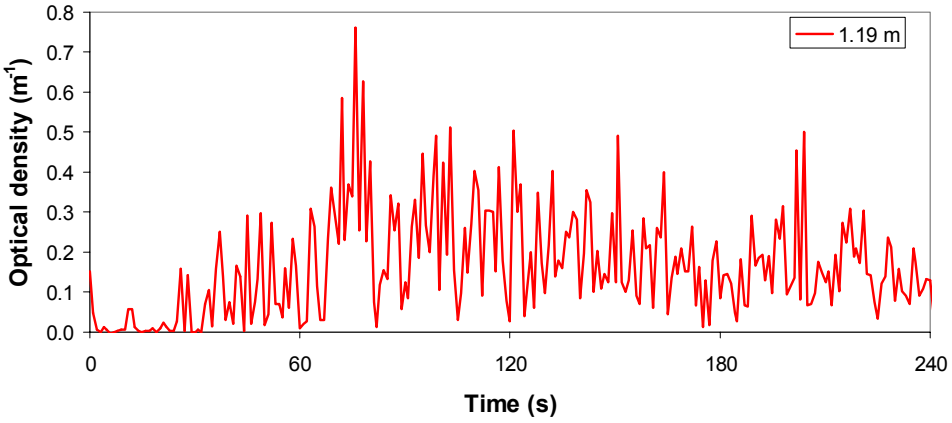

Figure 9 - Optical Density at 1.19 m (4 min emitter at Low Lighting)

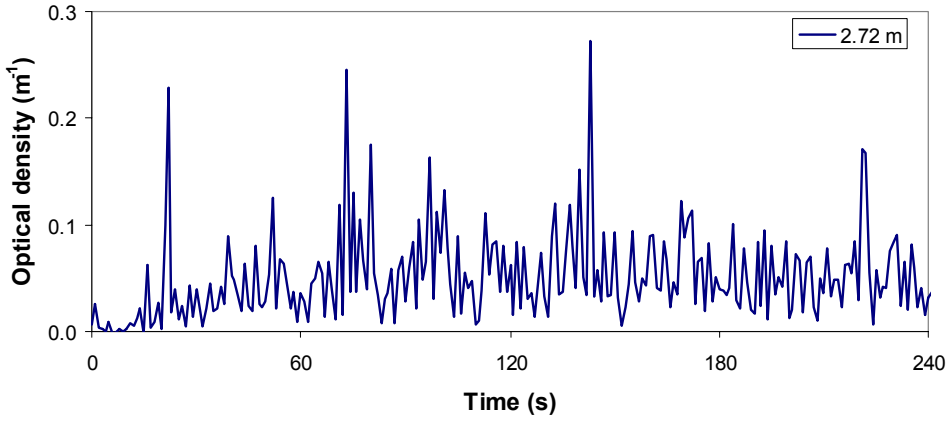

Figure 10 - Optical Density at 2.72 m (4 min emitter at Low Lighting)

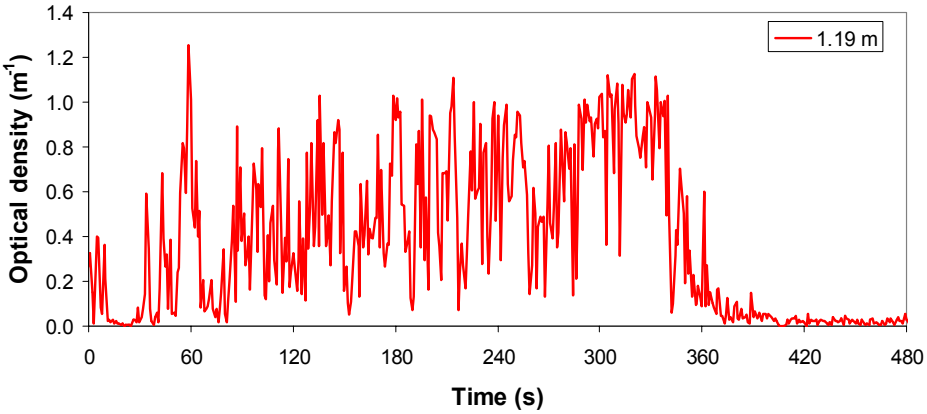

Figure 11 - Optical Density at 1.19 m (8 min emitter at Low Lighting)

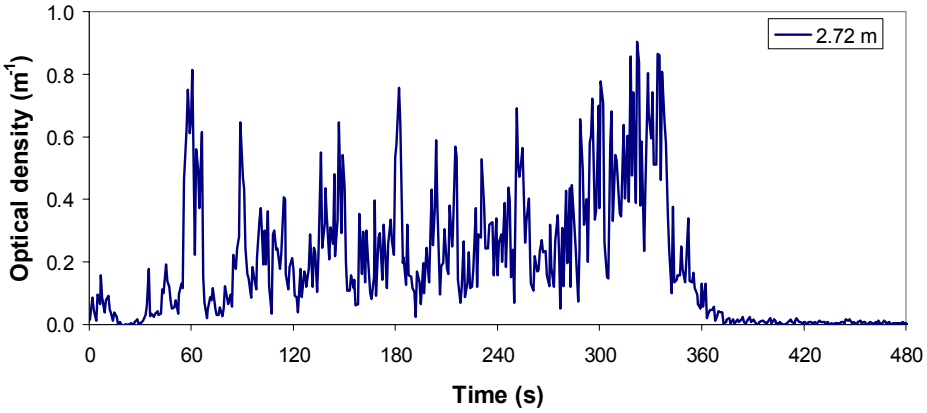

Figure 12 - Optical Density at 2.72 m (8 min emitter at Low Lighting)

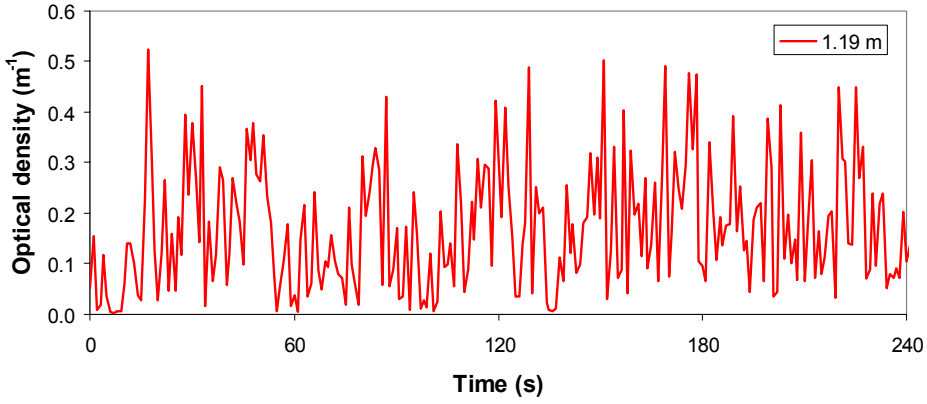

Figure 13 - Optical Density at 1.19 m (4 min emitter at High Lighting)

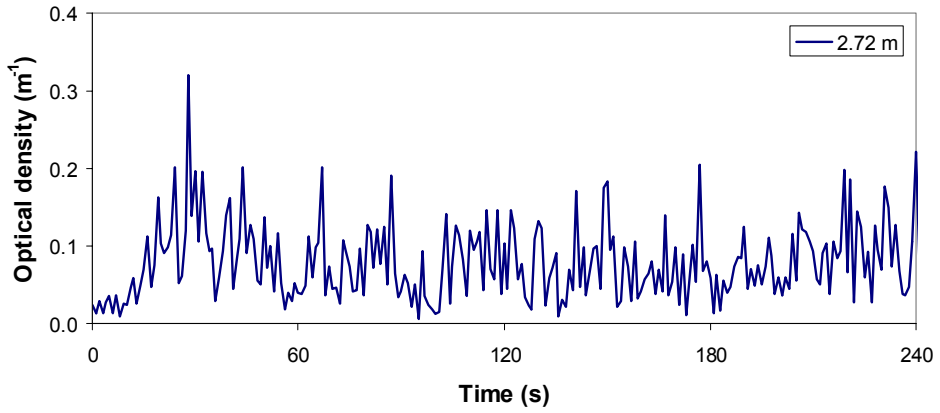

Figure 14 - Optical Density at 2.72 m (4 min emitter at High Lighting)

The centerline thermocouple measurements for each test are displayed in Figure 15 - Figure 17. One unforeseen issue with the radiant heaters that provided thermal lift for the smoke was that the heat output was cyclic rather than steady, as indicated by the variation in the temperature data. Similar to the optical density measurements, the temperature measurements show the effect of the air currents such that the highest four thermocouples did not have a large temperature difference. However, the thermocouples for the 4 minute emitter test under the high lighting condition each have a distinct temperature profile indicative of a plume that is centered along the thermocouple tree. The ambient temperature within Cole Field House was constant throughout the two days of testing at 20ºC (68ºF).

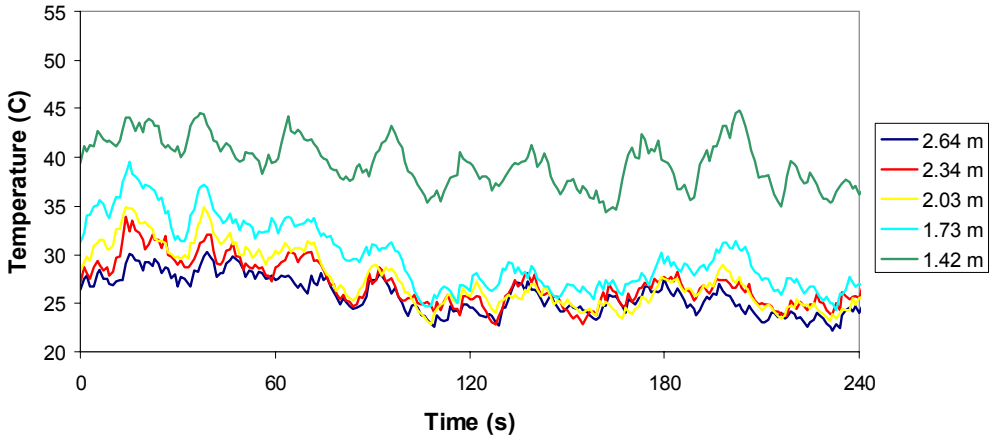

Figure 15 - Thermocouple Temperatures (4 min emitter at Low Lighting)

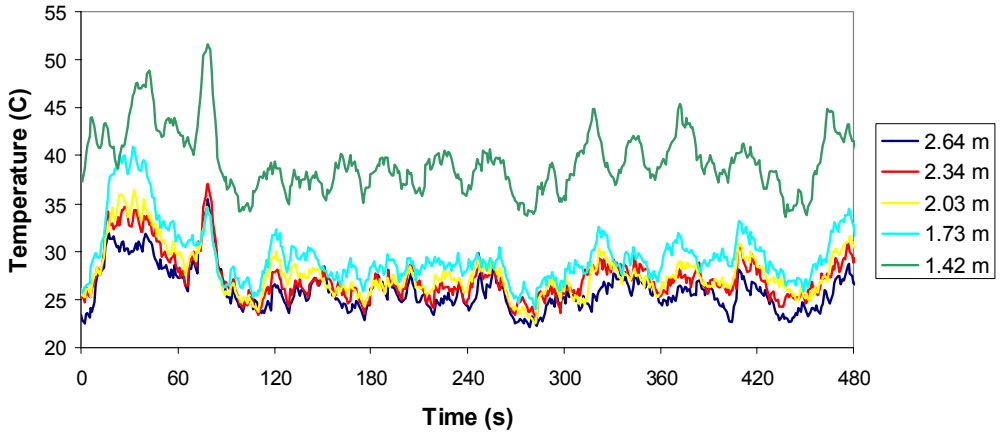

Figure 16 - Thermocouple Temperatures (8 min emitter at Low Lighting)

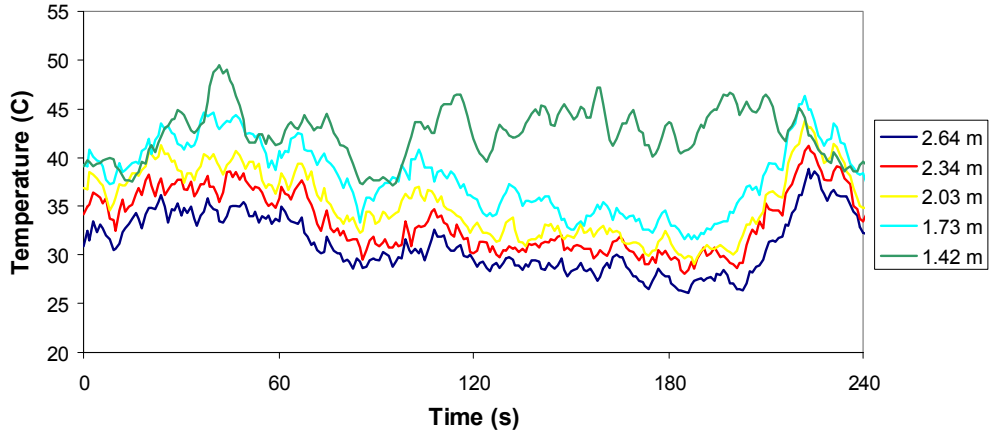

Figure 17 - Thermocouple Temperatures (4 min emitter at High Lighting)

5.3 Photometric Survey

Figure 18 displays the photometric survey locations for Cole Field House. The location of each measurement was taken at the intersection of a column and row as specified. The spacing of each column and row is approximately 7.6 m (25 ft). Additionally, Table 7 and Table 8 display the measurements for the low and high lighting levels respectively as well as Figure 19 and Figure 20 graphically depict the light intensity over the floor area.

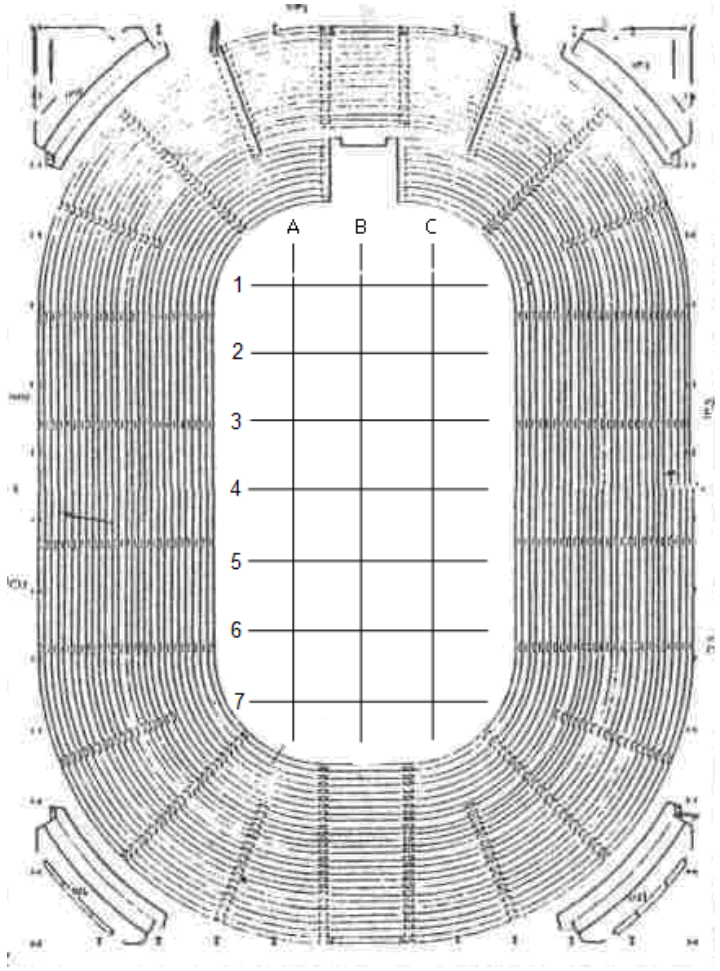

Figure 18 - Schematic of Photometric Survey Locations at Cole

Table 7 - Photometric Measurements taken at Low Lighting

Low lighting level (lux)			
	Columns		
Rows	A	B	C
1	88.2	92.5	94.7
2	181.8	188.3	186.1
3	335.7	337.9	329.3
4	-	401.3	-
5	297.0	292.7	305.6
6	173.2	173.2	173.2
7	85.0	87.2	80.7

*Conversion: 1 foot-candle = 10.76 lux

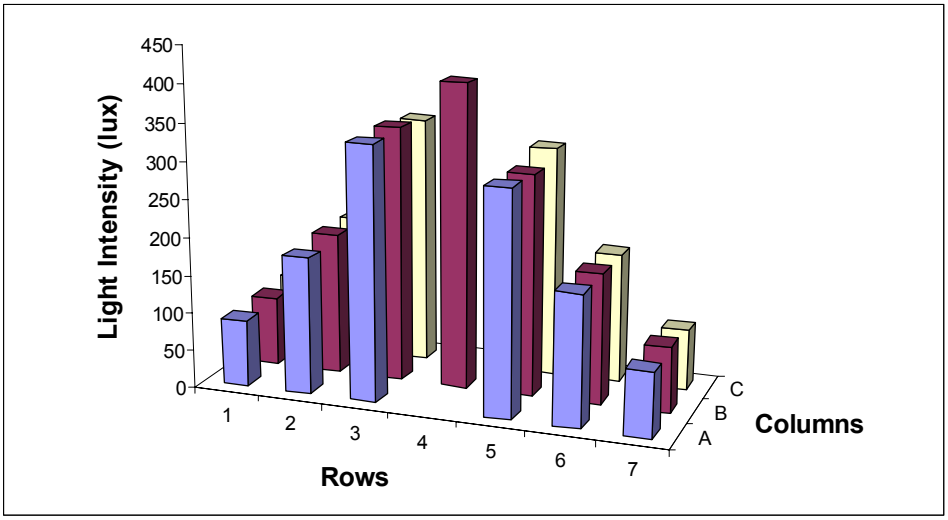

Figure 19 – Graphical Depiction of Photometric Measurements taken at Low Lighting

Table 8 - Photometric Measurements taken at High Lighting

High lighting level (lux)			
	Columns		
Rows	A	B	C
1	691.9	568.1	591.8
2	979.2	791.9	734.9
3	837.1	826.4	760.7
4	-	788.7	-
5	745.7	781.2	692.9
6	698.3	742.4	686.5
7	462.7	490.7	662.8

*Conversion: 1 foot-candle = 10.76 lux

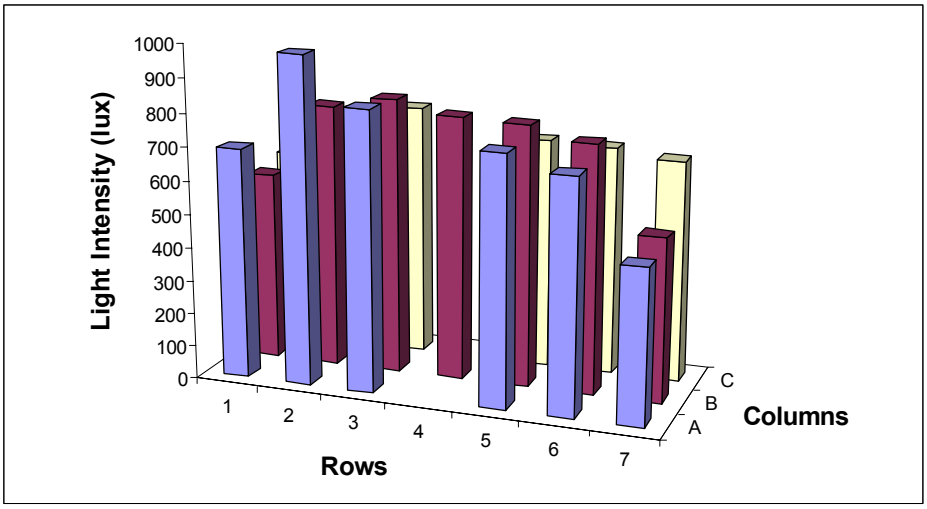

Figure 20 - Graphical Depiction of Photometric Measurements taken at High Lighting

6 Development of Predictive Algorithm

6.1 Qualitative Review of Data

A simple analysis was performed to assess the performance of the VID system for different lighting conditions as well as different backgrounds, both of which affect the visual contrast between the smoke plume and the background. From the list of detection times according to axonX's algorithm as displayed in Table 4 - Table 6, a comparison is made between the two lighting conditions (low and high) for the 4 minute tests to show the effect of the lighting conditions on activation times for each camera. Table 9 shows a comparison of the activation times at the two lighting levels.

Table 9 - Comparison of Activation Times for Different Lighting Levels for 4 min emitter

Location A Camera	Low level $t_{activation}$ (s)	High level $t_{activation}$ (s)	Low - High $\Delta t_{activation}$ (s)
1	27	28	-1
2	18	24	-6
3	31	21	10
4	25	40	-15
5	40	35	5
6	15	80	-65
7	23	30	-7
8	19	25	-6
AVG	25	36	-11

Overall, Table 9 shows that the VID system typically activated faster when the lighting level is at the lower level. The average difference in time to activation from the low lighting level to the high level for all eight cameras is 11 seconds. It is interesting to note that camera 3 and 5 activated sooner for a greater lighting level. However, the more perplexing result is that it took camera 6 an additional 65 seconds to activate for the

high lighting level. Based on the video images, this abnormality could be due to the effect of direct light impingement on the smoke along with a strongly illuminated background. Figure 21 shows the image from camera 6 one second prior to activation. The left image is at the low lighting level and the right image is at the high lighting level.

Figure 21 - Lighting Level Effect on Activation Time

Another comparison is made between two cameras that had a similar field of view of the source and background to show the dependence between the contrast of the plume compared to the background based on the same source and lighting condition.

Contrast can be defined as the difference, in color or tone, which makes an object distinguishable from other objects. In visual perception, contrast is determined by the difference in the color and brightness of the object with respect to other objects in the same FOV. Contrast is an important parameter for visual identification and is used by the Life Safety Code (NFPA 101) for exit signs. The contrast between the letters and background for an illuminated exit sign are designed to have a contrast ratio of not less than 0.5 and colors typically used to provide this threshold are red or green letters on matte white background. The contrast ratio is presented by Equation 7 [24].

$$Contrast = \frac{L_g - L_e}{L_g} \tag{7}$$

The distance to the source was kept constant for the specific cameras in comparison, which include the following pairs 2 & 8, 4 & 6, 1 & 5, and 3 & 7 (see Table 2). Figure 22 and Figure 23 show a comparison of the time to activation cameras with a relatively constant distance to the source for the same lighting condition (low) for the 4 minute smoke emitter. The backgrounds were similar for the camera pairs (see Figure 5).

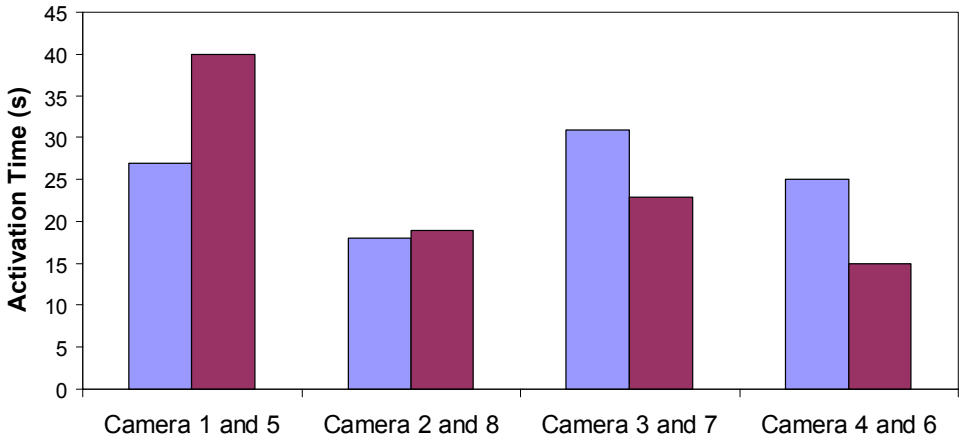

Figure 22 - Comparison of Activation Times at Low Lighting Level

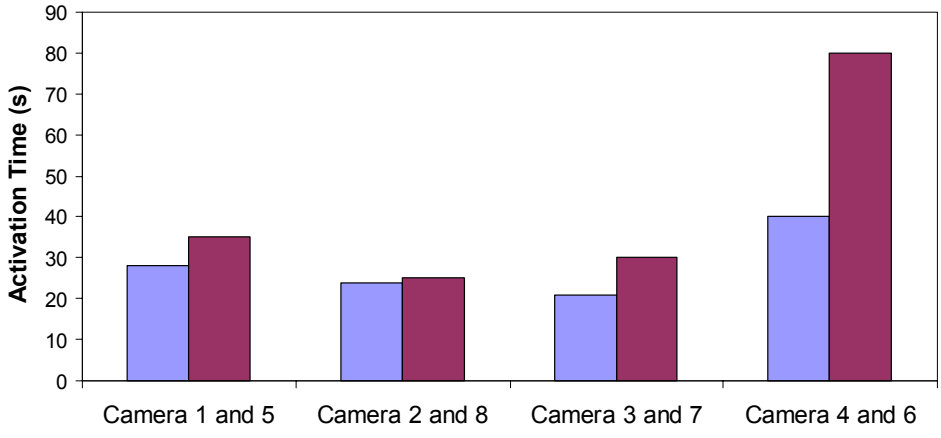

Figure 23 - Comparison of Activation Times at High Lighting Level

Overall, Figure 22 and Figure 23 show that the VID system has a dependence on the contrast of the smoke plume and background. The contrast between the smoke plume and background can be seen in the individual camera images shown by Figure 5. Camera 2 and 8 follow a consistent trend since both cameras provide almost a mirror image of each other. Camera 1 shows a darker background than camera 5 and therefore the quicker activation of camera 1 is expected. It is interesting that cameras 3 & 7 and cameras 4 & 6 flip with respect to a quicker time to activation when the lighting level increases.

6.2 Parameters of Interest

The ability to develop an algorithm to predict the activation time of a VID system to detect a smoke plume is dependent on several parameters that are based on fundamental principles of optics, which include luminance (an indicator of how bright an object will appear) and contrast. From observations and trends in the qualitative analysis in section 6.1, which reviewed the activation times with respect to the effect of lighting level and contrast, a more in-depth analysis of these two parameters is necessary to understand the relationship.

Another important parameter is the distance to the source location. The effect of distance to the source has a direct relationship on the size of the image reflected by each pixel. AxonX has indicated that their flame algorithm requires the fire to occupy a minimum of 6 x 6 pixels to detect a flame [4]. Similarly, there is no documented minimum number of pixels defined for a threshold with respect to activation for a smoke algorithm. Based on this premise, an additional relationship on the total number of pixels

enclosed by the smoke algorithm with respect to the overall amount of pixels in a standard image is incorporated.

A more useful parameter for defining a smoke plume is the plume volumetric flow rate $\left(\dot{V}_{pl}\right)$ as presented by Equation 5 in section 3.3. However, the determination of the volumetric plume flow rate is difficult to quantify when the VID system only has a two-dimensional view of the plume and over an entire height within the FOV (not just at a specific height as in the case of a beam detector). Even though the smoke production rate of the smoke emitters can be estimated, the prediction of the overall volume based on air entrainment is not a trivial plume property to quantify. Instead, an analysis of the optical density (δ) over the entire height in 1.5 m (5 ft) intervals of the arena is performed in section 6.3, "Optical Density Calculation" to show the large dependence on air entrainment with increasing height. Specifically, the 4 minute emitter test under the high lighting level was analyzed.

The plume outline growth rate for this analysis was based on the fraction of the pixels enclosed by the smoke algorithm with respect to the total number of pixels of the image divided by the activation time. This method was deemed the most practical based on the issue that the plume algorithm didn't necessarily enclose the entire smoke plume in the FOV. More often than not, the algorithm would detect only half of the plume at activation due to a dependence on contrast with respect to the bleachers and ceiling color. Figure 24 shows how the smoke algorithm (outline around smoke plume) would occasionally activate while the smoke was within the bleachers that were red and would not detect the smoke above the bleachers on the wall/ceiling that was an off white.

Figure 24 - Contrast Effect on Algorithm Activation

The four parameters of interest are designated with the following nomenclature throughout the analysis:

1) Photometric reading of light intensity (I)

2) Contrast between plume and background (C)

3) Distance to source from each camera (D)

4) Plume outline growth rate (G)

6.3 Optical Density Calculation

Measurements of the plume characteristics were made to characterize the source as well as the quality of smoke produced. The two measurements taken were plume centerline temperature and optical density. From the plume centerline temperature measurements, the heat release rate (HRR) was determined and further used to predict the volumetric plume rate. The two optical density measurements along with the HRR and volumetric plume rate were used to then determine the fuel parameter term from Equation 6 in section 3.3. The determination of the fuel parameter from the obscuration measurements taken at the two heights allows the optical density of the plume to be estimated at a range of heights.

The 4 minute emitter test under the high lighting level is used throughout this calculation due to the better data taken by the optical density measurement and centerline thermocouples above the source (smoke source was aligned according to air currents such that the smoke plume would rise through the two beams of light and within the thermocouple tree).

Based on the centerline temperature data taken as shown in Figure 17, the HRR was estimated by applying a plume centerline temperature correlation developed by Heskestad as presented in section 3.3, Equation 2. For the purposes of estimating a HRR from a characteristic temperature at a particular height, an average temperature was taken for each thermocouple over the test duration.

From the experimental observations, the two highest thermocouples located at 2.64 m (8.66 ft) and 2.34 m (7.68 ft) were within the plume with average temperatures of 304.2K and 306.5K, respectively. Since Heskestad's equation has two unknowns (HRR and z_0), a process of solving two equations with the respective two unknowns was performed from the temperature data at the two highest thermocouples as shown by Equation (8 and 9).

$$304.2K = 25\dot{Q}_c^{2/3}\left(2.64m - z_0\right)^{-5/3} + 293K \qquad (8)$$

$$306.5K = 25\dot{Q}_c^{2/3}\left(2.34m - z_0\right)^{-5/3} + 293K \qquad (9)$$

Solving Equation 8 and 9 simultaneously resulted in the convective portion of the HRR, $\dot{Q}_c = 4.02\,\text{kW}$ (3.81 Btu/s)[2] and the characteristic HRR, $\dot{Q} = 5.74\,\text{kW}$ (5.44 Btu/s). In addition, the virtual origin was determined to be -0.18 m (-7.09 in). This characteristic HRR is used in the plume entrainment rate and plume property estimates provided in the remainder of this calculation.

The total heat output of the radiant heaters of 26.4 kW was shown to be an inefficient way to provide thermal buoyancy to the smoke plume compared to the calculated HRR of 5.74 kW. Approximately 1/5 of the total heat output from the burners was directed into the smoke plume.

Based on the calculated HRR, the volumetric plume rate is determined from the plume mass entrainment rate by Heskestad's correlation as presented in section 3.3 from Equation 4. The volumetric plume flow rate is determined at the two ODM locations, i.e. at 1.19 m (3.90 ft) and 2.72 m (8.92 ft) above the source. The plume volumetric flow rate can be calculated from the plume mass entrainment rate from Equation 5. Being that the plume temperature is not significantly different from the ambient air temperature based on the small fire source and temperature measurements, the plume density (ρ_{pl}) is evaluated at the normal density of air, 1.2 kg/m^3 (0.0749 lb/ft^3). The results from Heskestad's correlation are shown in Table 10.

Table 10 - Calculated $\dot{V}$ from Mass Plume Entrainment Correlations for Heskestad

z (m)	$\dot{m}_{pl}$ (kg/s)	$\dot{V}$ (m^3/s)
1.19	0.183	0.153
2.72	0.658	0.548

*Conversion: 1 m = 3.281 ft, 1 kg = 2.205 lb, 1 m^3 = 35.31 ft^3

[2] The convective portion of the heat release rate is assumed to be 70% of the total heat release rate.

Using the two optical density (δ) measurements taken at 1.19 m (3.90 ft) and 2.72 m (8.92 ft) above the source, the calculated HRR, and the plume volumetric flow rate, a fuel parameter (mass optical density (δ_m) divided by the effective heat of combustion) can be determined from Equation 6 in order to characterize the smoke source.

Applying this fuel parameter determined from the obscuration measurements taken at the two heights allows the optical density of the plume to be estimated at a range of heights. The data from Figure 13 shows a great deal of fluctuation for the measurement at 1.19 m (3.90 ft) due to the movement of the plume in and out of the light beam due to modest air currents in the vicinity of the source. Because of these fluctuations, the data was evaluated over a broad time and includes high peaks and moderate peaks from 0.50 m^{-1} to 0.30 m^{-1} (0.15 ft^{-1} to 0.09 ft^{-1}) to indicate the overall range of the fuel parameter. Similarly, the data from Figure 14 shows less variation due to the smoke being consistently intercepted by the light beam optical density for the measurement at 2.72 m (8.92 ft), however the small fluctuation in peaks from 0.20 m^{-1} to 0.10 m^{-1} (0.06 ft^{-1} to 0.03 ft^{-1}) are also evaluated for consistency.

Table 11 displays the calculated fuel parameter over the range of optical densities specified for both ODM locations from Equation 6. A sample calculation of the fuel parameter based on the measurement at an elevation of 1.19 m (3.90 ft) above the source, with an optical density of 0.50 m^{-1} (0.15 ft^{-1}), is presented as Equation 10.

$$\frac{\delta}{\left(\frac{\dot{Q}_c}{\dot{V}_{pl}}\right)} = \left(\frac{\delta_m}{\chi_a \Delta H_f}\right) = \frac{0.50\, m^{-1}}{\left(\frac{4.02\, kW}{0.153\, m^3/s}\right)} = 0.019 \text{ m}^2\text{/kJ } (0.216 \text{ ft}^2\text{/Btu}) \qquad (10)$$

Table 11 - Fuel Parameter Estimation from Optical Density

z (m)	High δ (m^{-1})	Moderate δ (m^{-1})	High FP (m^2/kJ)	Moderate FP (m^2/kJ)
1.19	0.50	0.30	0.019	0.011
2.72	0.20	0.10	0.027	0.014

* Conversion: 1 m^{-1} = 0.305 ft^{-1}, 1 m^2 = 10.76 ft^2, 1 kJ = 0.9478 Btu

Good agreement was obtained for the estimates of the fuel parameter at the two different elevations over the range of fluctuations during the time that the smoke plume was being present in the light beam. A value in the range of 0.019 to 0.014 m^2/kJ (0.216 to 0.159 ft^2/Btu) can be evaluated to estimate the range of optical density expected in the plume at a given height. Table 12 lists the optical density for a range of heights of interest at Cole Field House for the high and low range of the calculated fuel parameter. Table 12 shows how dramatically the volumetric plume flow rate and optical density are dependent on the air entrainment with increasing height.

Table 12 - Optical Density at Varying Height and Range of Fuel Parameter

z (m)	$\dot{m}_{pl}$ (kg/s)	$\dot{V}$ (m^3/s)	FP = 0.019 $\delta\,(m^{-1})$	FP = 0.014 $\delta\,(m^{-1})$
3.0	0.769	0.641	0.119	0.088
4.5	1.471	1.225	0.062	0.046
6.0	2.342	1.952	0.039	0.029
7.5	3.367	2.806	0.027	0.020
9.0	4.536	3.780	0.020	0.015
10.5	5.840	4.866	0.016	0.012
12.0	7.271	6.060	0.013	0.009
13.5	8.826	7.355	0.010	0.008
15.0	10.499	8.749	0.009	0.006
16.5	12.285	10.238	0.007	0.005
18.0	14.183	11.819	0.006	0.005
19.5	16.187	13.489	0.006	0.004
21.0	18.296	15.247	0.005	0.004
22.5	20.507	17.089	0.004	0.003
24.0	22.818	19.015	0.004	0.003
25.5	25.227	21.022	0.004	0.003
27.0	27.731	23.109	0.003	0.002
28.5	30.329	25.274	0.003	0.002
30.0	33.019	27.516	0.003	0.002

*Conversion: 1 m = 3.281 ft, 1 kg = 2.205 lb, 1 m^3 = 35.31 ft^3, 1 m^{-1} = 0.305 ft^{-1}

6.4 Normalization of Time

The detection time of the SigniFire system was dependent on when the smoke came into the FOV of the image. Based on the overall FOV of each camera at location A, the time at which the smoke source entered in the FOV was dependent on the height of the FOV above the source. This was also a direct relationship with the proximity of the camera to the testing location. With the intent to be as consistent as possible based on the four parameters, a calculation was completed to properly correlate a normalized activation time based on the SigniFire detection time.

Camera 1 and 5 where the only cameras in which the smoke started in the FOV, whereas the FOV of the remainder of the cameras was above the smoke source. The

height of the FOV above the source was estimated with respect to a known height, i.e. ODMs on the structure of the instrumentation apparatus. Based on the reference objects, a time delay for the plume to become visible in the FOV was calculated from a plume lag correlation.

Based on the HRR calculations from section 6.3, the lag time of the plume was determined from Mowrer's plume lag time correlation as presented in section 3.3 from Equation 3 for a steady fire. From the images at each camera, an estimation of the height of the bottom portion of the FOV above the source was determined from the height of the two ODMs, i.e. at 1.19 m (3.90 ft) and 2.72 m (8.92 ft) above the source. Cameras 3 and 7 did not show the measurement apparatus and was therefore calculated based on trigonometry from images.

The plume lag time results are shown in Table 13 along with the height estimations above the source.

Table 13 –Time to Enter FOV

Camera	Height (m)	t_{delay} (s)
1	0	0.0
2	2	0.9
3	4	2.4
4	3	1.6
5	1	0.4
6	3	1.6
7	4	2.4
8	0	0.0

The normalized times for the analysis are displayed in Table 14 through Table 16 as shown by $t_{activation}$* for all eight cameras and sources conducted at Cole Field House. The normalization of the activation time provided a consistent analysis and is presented as Equation 11.

$t_{activation}$* = algorithm activation time (VID) – time for smoke to enter FOV (11)

Table 14 – Normalized Activation Time for 4 min emitter at Low Lighting

4 min (Low Lighting level)			
Camera	Alarm	$t_{activation}$ (s)	$t_{activation}$* (s)
1	Smoke	27	27
2	Smoke	18	17
3	Smoke	31	28
4	Smoke	25	23
5	Smoke	40	39
6	Smoke	15	13
7	Smoke	23	20
8	Smoke	19	19

Table 15 – Normalized Activation Time for 8 min emitter at Low Lighting

8 min (Low Lighting level)			
Camera	Alarm	$t_{activation}$ (s)	$t_{activation}$* (s)
1	Smoke	16	16
2	Smoke	15	14
3	Smoke	17	14
4	Smoke	148	146
5	Smoke	15	14
6	Smoke	41	39
7	Smoke	13	10
8	Smoke	16	16

*The smoke emitter stops production smoke at 17 seconds and restarts at 30 seconds

Table 16 - Normalized Activation Time for 4 min emitter at High Lighting

4 min (High Lighting level)			
Camera	Alarm	$t_{activation}$ (s)	$t_{activation}$* (s)
1	Smoke	28	28
2	Smoke	24	23
3	Smoke	21	18
4	Smoke	40	38
5	Smoke	35	34
6	Smoke	80	78
7	Smoke	30	27
8	Smoke	25	25

6.5 Analysis

The four parameters of interest are discussed here more in depth with respect to the methodology for determining the input values for the analysis. The photometric survey taken at ground level of the arena floor was shown to have a large variation depending on the direct light impingement from the metal halide lights. The values used for the analysis were based on the average values of 205.6 lux (19.1 foot-candles) at the low lighting level 712.6 lux (66.2 foot-candles) for the high lighting level. The process of adopting a light level intensity for a particular camera based on the local lighting intensity levels associated with the camera was not used due to the unknown ability of the cameras to process light over the length of the arena floor area.

The contrast between the plume and background initially showed an important relationship for activation time. The process to estimate the contrast was based on the measurement of luminance for both the smoke plume and adjacent background. Still images were used from the archived video images for the analysis. The archived video was recorded in grayscale. It is interesting to note that the SigniFire processor only looks at the grayscale images to help minimize nuisance sources with respect to bright colors [16]. The software used to measure the contrast was by an image analysis software, Spotlight-8 [25]. A repetitive process of using a feature of the software known as the area of interest (AOI) and the option of "new" followed by "line profile" set at a "line width" of 4 gave the ability to measure the luminance of the desired area at a good resolution.

The image at activation was used as a baseline to ensure a consistent plume measurement. The only area of concern of the plume was that which was enclosed by the

algorithm. At activation, the plume algorithm from the SigniFire system would outline the smoke plume. An additional image at one second prior to activation was used for the measurement. The measurement was taken within the boundaries of the plume algorithm outline at activation for the plume measurement or adjacent to the plume following the overall plume height for the background measurement. The main reason to back up one second was that luminance measurements taken at activation were skewed due to the bright outline of the smoke algorithm. This image just prior to activation is considered to give a reasonable estimate of the contrast ratio threshold at the time of activation.

The plume luminance measurement at one second prior to activation is based on the amount of the plume enclosed by the smoke algorithm. Three measurements were taken within the smoke algorithm to generate an overall average luminance of the smoke plume. The measurements were taken along the presumed centerline, between the left edge and centerline, and between the right edge and centerline of the plume. The values were then averaged and used as the luminance value for the plume.

Similarly, the measurement of the background (stadium seating and wall/ceiling) was taken on the same image at one second prior to activation. A measurement was taken along a line close to the right and left side of the plume which followed the entire plume algorithm outline. The values were then averaged and used as the luminance value for the background. This two image measurement process discussed for both the plume and background luminance is shown in Figure 25.

Figure 25 - Images used to Determine Contrast Ratio

Based on the luminance values determined for the plume and background, the contrast ratio was determined from Equation 7 presented in section 6.1. The measurements revealed that the smoke always had a greater luminance than the background due to the grayish-white color.

The contrast ratios determined for all three sources are listed in Table 17 - Table 19. The ranges are 0.28 – 0.50 for the 4 min emitter at a low lighting level, 0.30 - 0.60 for the 8 min emitter at a low lighting level, and 0.28 – 0.44 for the 4 min emitter at a high lighting level. The overall ranges are within a close range which shows a general dependence for contrast threshold. Additionally, Figure 26 displays the contrast ratio trends for each test and camera.

Table 17 - Contrast Ratio for 4 min emitter at Low Lighting

4 min (Low lighting level)	
Camera	Contrast ratio
1	0.41
2	0.40
3	0.43
4	0.50
5	0.39
6	0.28
7	0.31
8	0.31

Table 18 - Contrast Ratio for 8 min emitter at Low Lighting

8 min (Low lighting level)	
Camera	Contrast ratio
1	0.43
2	0.49
3	0.46
4	0.60
5	0.45
6	0.30
7	0.35
8	0.44

Table 19 - Contrast Ratio for 4 min emitter at High Lighting

4 min (High lighting level)	
Camera	Contrast ratio
1	0.42
2	0.33
3	0.35
4	0.41
5	0.44
6	0.31
7	0.28
8	0.32

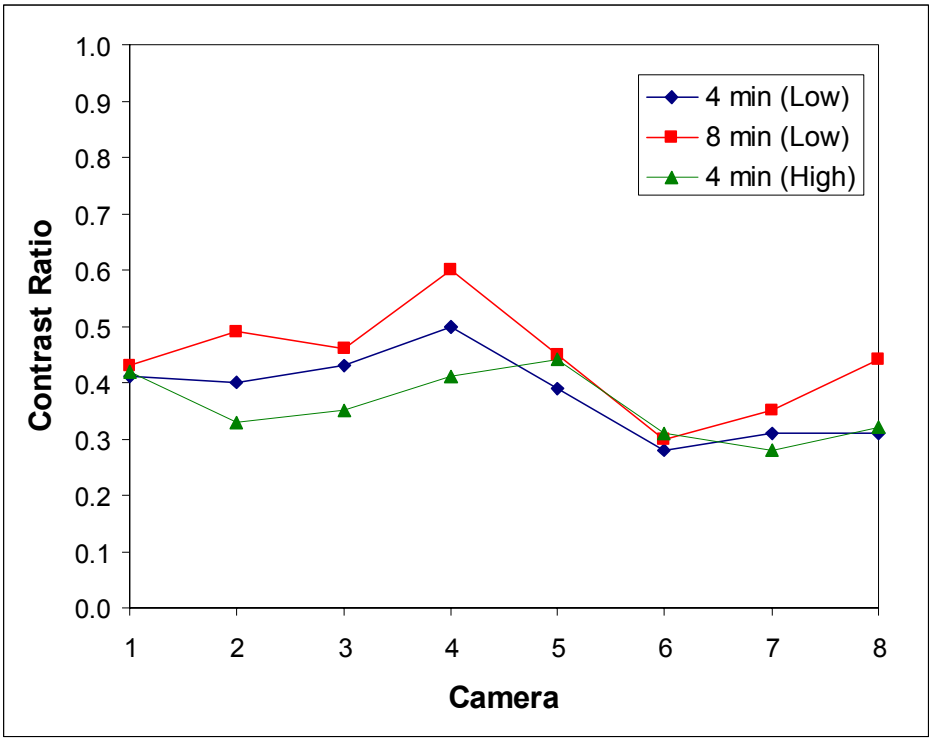

Figure 26 - Contrast Ratio for Three Tests and Eight Cameras

The distance to the source from each camera is known to have a direct relationship with the pixel spacing in the object plane. The distance to the source at location A from each camera was determined from an original blueprint drawing of Cole Field House from UMD's facilities archive building and displayed in Table 2.

One of the difficulties with analyzing the image in two dimensions is the ability to quantify the plume volumetric flow. Instead of this parameter, a plume outline growth rate is implemented and determined from the fraction of the pixels enclosed by the smoke algorithm with respect to the total number of pixels. The fraction of the pixels is calculated as the percentage of the overall image divided by the normalized activation time. The percentage of the overall image was used with the intent to remove the effect of distance from this parameter. The number of pixels enclosed by the algorithm is determined by an image analysis software, Adobe Photoshop. A process of using the "magic wand" tool to outline the plume algorithm and then the process of changing all the pixels within the outline (plume) to white and everything else (background) to black gave the ability to then use another image software program to count the pixels. Figure 27 shows a "before" and "after" picture for the analysis procedure.

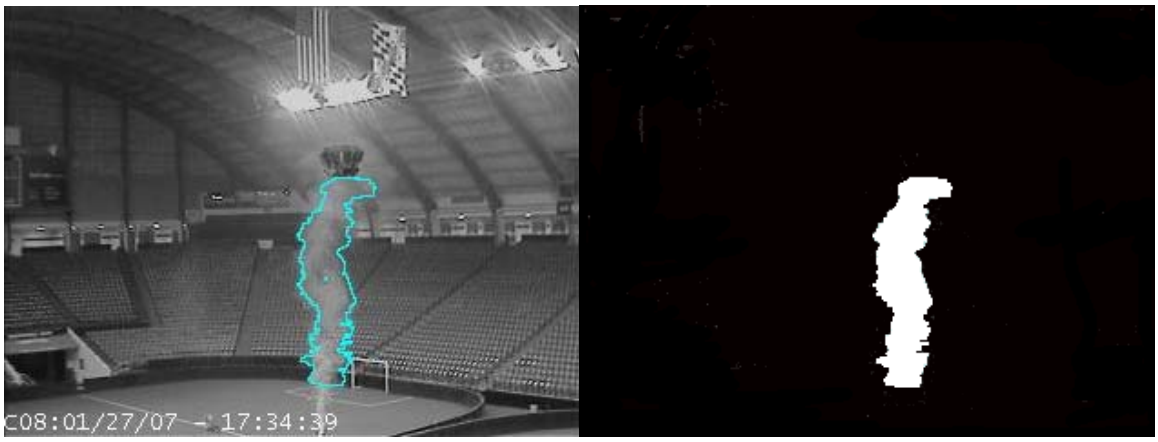

Figure 27 - Pixel Count Process Before and After

The second program used to count the pixels was Spotlight-8. A repetitive process of using an area of interest (AOI) and the option of "new" followed by "rectangle" gave the option to draw a rectangle around the plume which then allowed a process to count the pixels that were white. After the rectangle is drawn around the plume, the total number of pixels encompassed by the plume is determined by the software. The "process" display field at the top of the information bar is selected followed by "statistics" and lastly the "area (of threshold white pixels)". The number of pixels enclosed within the algorithm is divided by the total number of pixels in the image (76,800). The resulting number is calculated as a percent and then divided by the normalized time to activation. The plume outline growth rate measurements for all three sources are listed in Table 20 - Table 22.

Table 20 - Plume Outline Growth Rate for 4 min emitter at Low Lighting

4 min (Low lighting level)	
Camera	Pixel Growth (s^{-1})
1	0.10
2	0.35
3	0.49
4	0.26
5	0.32
6	0.49
7	0.24
8	0.17

Table 21 - Plume Outline Growth Rate for 8 min emitter at Low Lighting

8 min (Low lighting level)	
Camera	Pixel Growth (s^{-1})
1	0.17
2	0.46
3	0.84
4	0.16
5	0.53
6	0.12
7	0.70
8	0.28

Table 22 - Plume Outline Growth Rate for 4 min emitter at High Lighting

4 min (High lighting level)	
Camera	Pixel Growth (s^{-1})
1	0.13
2	0.23
3	0.38
4	0.32
5	0.21
6	0.17
7	0.19
8	0.14

6.6 Results

The ability to develop an algorithm to predict the activation time for a smoke plume is dependent on the four parameters of interest. A multi-variable regression analysis was performed to correlate values for the independent variables (four parameters) into a relationship for the dependent variable (activation time). A power law analysis was correlated due to the expectation of the parameters to follow a power law trend. Performing the regression analysis for a prediction of the time to activation through Microsoft Excel results in Equation 12.

$$t_{correlated} = 16075 \frac{I^{0.185} C^{1.311}}{D^{1.927} G^{0.810}} \tag{12}$$

Figure 28 displays the activation time for the experiments (y-axis) compared to the predicted time from the regression analysis (x-axis) as a log-log plot. The ideal plot is depicted as the solid line in the figure. Additionally, the bands of ±30% are displayed as dashed lines. An under prediction of the activation time by the correlation results in a data point above the best fit line, and an over prediction is below the best fit line.

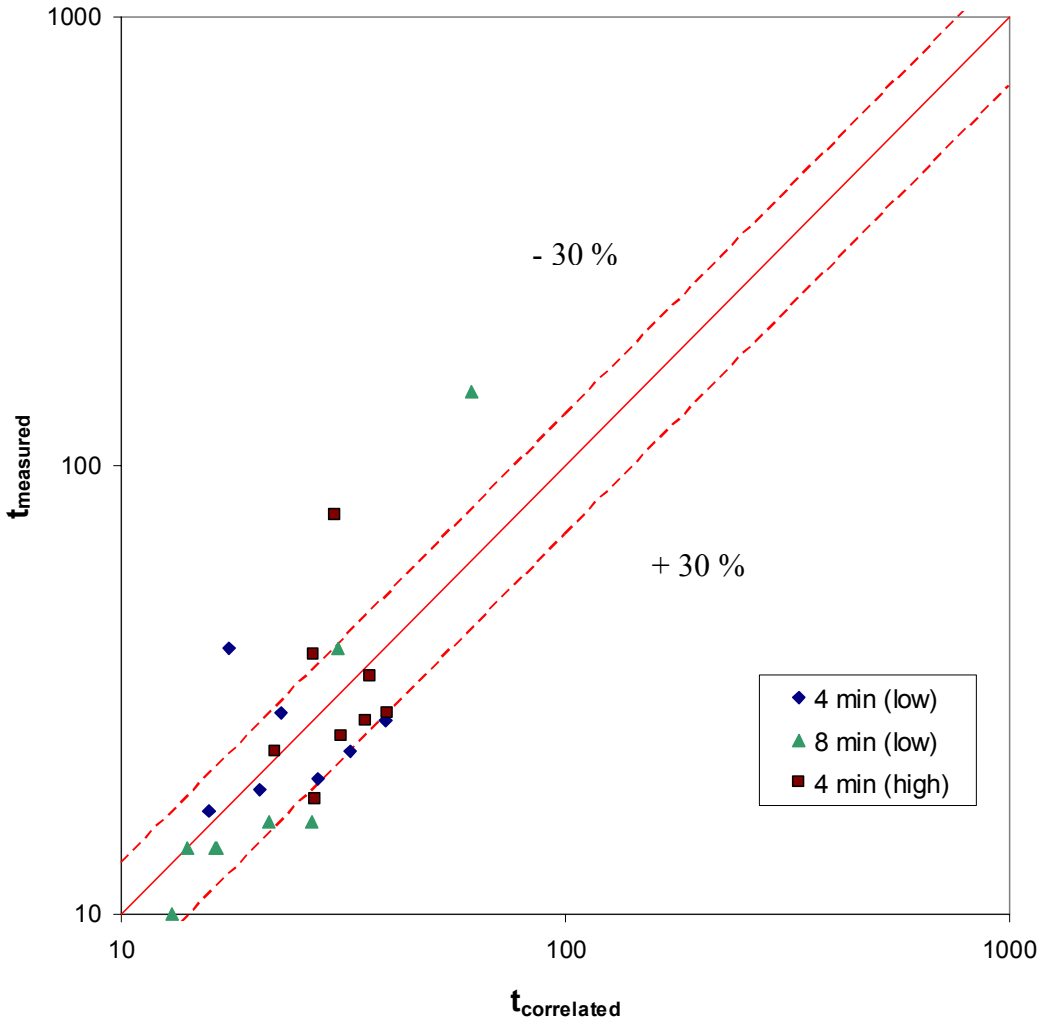

Figure 28 - Regression Analysis of Experimental versus Predicted Time to Activation

The statistical output from the regression analysis is displayed in Table 23. The "Multiple R" commonly known as the multiple correlation coefficient is the correlation between the y (experimental results) and $\hat{y}$ (predicted results). The R = 0.722 indicates that the y and $\hat{y}$ are moderately correlated [26]. The "R Square" measures the proportion of total variation about the mean $\overline{Y}$ explained by the regression. The $R^2 = 0.521$ indicates that 52.1% of the total variation in time may be explained by the regression line relating

this variable to the number of parameters. This implies that 47.9% of the variation is unexplained by the correlation. The low value associated with R^2 shows that there is an appreciable amount of variation about the correlated equation. The "Standard Error" measures the standard deviation of the residuals. The residual is the "difference between the observed values of y and the predicted values based on the regression equation" [26] as shown by Equation 12.

Table 23 - Regression Analysis Statistical Output

Regression Statistics	
Multiple R	0.722
R Square	0.521
Standard Error	0.454

Table 24 provides a summary of the role of each of the individual parameters in the analysis. The coefficients show the dependence of each parameter on the overall activation time as displayed in Equation 12. The remaining columns describe the significance of each coefficient in the model, i.e., different than zero. The "Standard Error" column displays the standard deviation of each coefficient. The "t Stat" column "shows how many standard deviations the observed coefficient is from zero" [26] which is the coefficient divided by the standard error. The most descriptive components of the table are the "P-value" and 95 % confidence intervals. A "P-value" is the "area in the tail of a t distribution beyond the computed t value" [26]. For experimental work, a P-value of "less than 0.05 is accepted as an indication that the coefficient is significantly different than zero" [26]. All of the parameters in the model have significant P-values except for the lighting level parameter. Additionally, the 95% confidence interval provides an indication if the coefficient may be zero. If the confidence interval includes zero, then the coefficient is not significant (i.e., not significantly different from zero) [26].

Furthermore, a wide range of values for the confidence interval implies that the coefficient is not well known. Similarly to the P-value conclusion, the lighting level parameter indicates that it may be zero and therefore have no effect on the prediction of activation time. The coefficient of 16075 ($e^{9.685}$) in the correlation relates specifically to the intercept term in Table 24.

Table 24 - Confidence of Regression Coefficients

	Coefficients	Standard Error	t Stat	P-value	Lower 95%	Upper 95%
Intercept	9.685	3.736	2.592	0.018	1.864	17.505
LN (I)	0.185	0.173	1.071	0.298	-0.177	0.547
LN (C)	1.311	0.528	2.482	0.023	0.205	2.417
LN (D)	-1.927	0.918	-2.100	0.049	-3.848	-0.006
LN (G)	-0.810	0.210	-3.850	0.001	-1.250	-0.370

The ANOVA (Analysis Of Variance) output as shown in Table 25 examines the hypothesis that the variation explained by the correlation from the regression analysis is zero. If this is true, then the prediction provided by the model could be equally well explained by chance alone. Table 25 is a single factor ANOVA table. The typical procedure of an ANOVA analysis is to state the null and alternative hypothesis, where H_o (all means are equal) versus H_A (at least three of the means are different).

The row labeled "Regression" is the source of variation between the groups and the row labeled "Residual" is the variation within a group. The column labeled "df" is degrees of freedom, "SS" is sum of squares, and "MS" is the mean square. One of the measures from an ANOVA that is important is the column in the table labeled "Significance F", which indicates the probability of getting the results due to chance alone. The value of 0.005 implies "that the probability of getting these results due to chance alone is less than 0.01" [26] for the entire model as a whole. Similarly, the "F" value can be compared at a significance level of $\alpha = 0.05\,(95\%)$ to determine if each

parameter produces different results. The critical F value based on the degrees of freedom results in $F_{.95}(4,19) = 2.90$. Since 5.168 > 2.90, the null hypothesis is rejected and can conclude that the parameters of interest are different for this analysis [26].

Table 25 - ANOVA Statistical Output

	df	SS	MS	F	Significance F
Regression	4	4.253	1.063	5.168	0.005
Residual	19	3.909	0.206		
Total	23	8.162			

From the statistical analysis, the effect of lighting level has relatively no effect based on the data from the P-value and 95% confidence interval. The result is understood due to the cameras having an auto-iris, which compensates for brightness in the image even though a large difference in light intensity was included in the test program.

Given the limited influence of the lighting level, a new multi-variable regression analysis was performed from the three statistically significant parameters (C, D, and G) and the resulting equation is presented as Equation 13.

$$t_{correlated} = 54830 \frac{C^{1.184}}{D^{2.023}\, G^{0.870}} \tag{13}$$

Figure 29 displays the activation time for the experiments (y-axis) compared to the predicted time from the regression analysis (x-axis) for the modified equation.

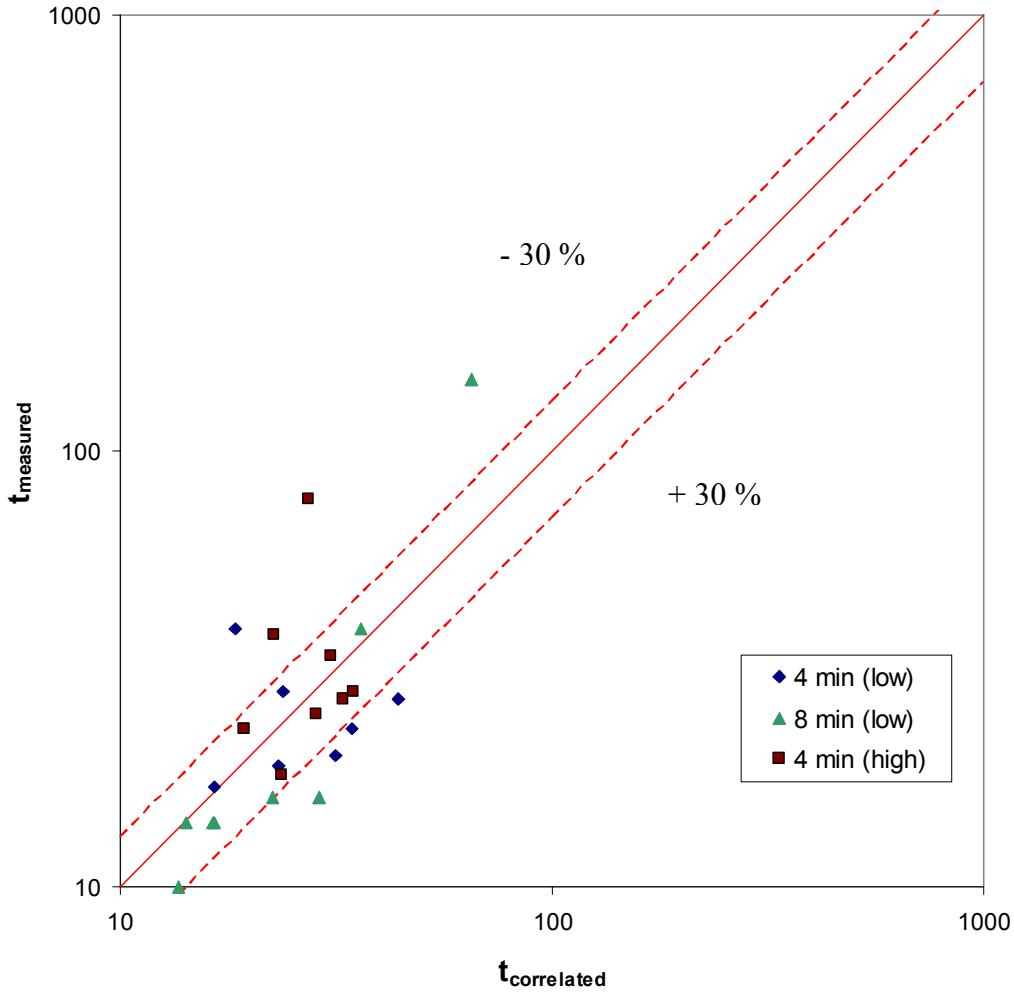

Figure 29 - Regression Analysis of Experimental versus Predicted Time to Activation (Modified)

The statistical output from the regression analysis for Equation 13 is displayed in Table 26. Table 27 provides a summary of the role of each of the individual parameters in the analysis. Lastly, Table 28 examines the hypothesis that the variation explained by the correlation from the regression analysis is zero. The critical F value based on the degrees of freedom results in $F_{.95}(3,20) = 3.10$.

Table 26 - Regression Analysis Statistical Output (Modified)

Regression Statistics	
Multiple R	0.702
R Square	0.492
Standard Error	0.455

Table 27 - Confidence of Regression Coefficients (Modified)

	Coefficients	Standard Error	t Stat	P-value	Lower 95%	Upper 95%
Intercept	10.912	3.569	3.058	0.006	3.468	18.357
LN (C)	1.184	0.517	2.292	0.033	0.106	2.262
LN (D)	-2.023	0.917	-2.207	0.039	-3.935	-0.111
LN (G)	-0.870	0.203	-4.277	0.000	-1.295	-0.446

Table 28 - ANOVA Statistical Output (Modified)

	df	SS	MS	F	Significance F
Regression	3	4.017	1.339	6.461	0.003
Residual	20	4.145	0.207		
Total	23	8.162			

Equation 13 is slightly more statistically significant than Equation 12, but shows more variation in Figure 29. In addition, each of the three parameters has a more refined coefficient. Given the limited range in parameters and limited number of tests, the power law coefficients for the predictive algorithm indicate general trends of each parameter.

The coefficient for contrast ratio indicates that as the contrast between the plume and background for the ranges measured (0.28 – 0.60) increases, the time to activation increases. This is counterintuitive because as contrast increases, the image has more resolution and a clearer definition between objects and the background. A contrast ratio of 1.0 is representative of a white object on a black background or vice versa, which would be expected to be promptly detected. This counterintuitive trend could be due to the effect that an opaque smoke plume (more optically dense) may not give as much of the plume changing characteristics as a thin, transparent smoke plume. The SigniFire algorithm may look at time varying plume characteristics for detection.

The coefficient for distance shows an inverse square relationship for the range of (37.8 m to 54.9 m (124 ft to 180 ft)). This implies that as distance increases away from the source, the time to activation decreases. This could be due because the SigniFire system may be able to capture the overall movement of the plume better at further distances. This would be the equivalent to a person looking at a small portion of the smoke plume through a small hole (representative of a close distance) and then looking at the entire smoke plume without any visual obstructions. The later method would allow a person to see the entire plume and the representative characteristics of its growth and movement for an easier and quicker depiction of the image.

Lastly, the coefficient for pixel growth rate implies that as the growth rate increases, the time to activation decreases. This trend seems intuitively correct because a faster developing plume (i.e., larger HRR) would allow the SigniFire system to see characteristics of the plume formation in a shorter time period.

It is important to discuss that an extrapolation of the data outside of the ranges tested may not follow the trends observed. Further testing is important to understand the dependence of each parameter over a much larger range of data.

7 Conclusion

The ability of the predictive algorithm to determine the time to activation is statistically significant. The overall trends for each parameter are reasonable based on the small data ranges of each parameter and limited number of tests. A wider range of data and in particular repeated tests would have given the ability to produce an improved algorithm with the ability to compensate for anomalies in individual tests. From the thermocouple data and applying Heskestad's correlations gave the ability to determine the HRR from the propane burners. In addition, an estimate of the transport lag time of the smoke plume was useful for developing a consistent method to compare activation times. Lastly, the optical density data gave the ability to estimate the optical density of the smoke plume to show the difficulty in quantifying the plume volumetric growth rate as a parameter of interest.

8 Future Research

Based on the results and issues with trying to normalize each camera's activation time, a few ideas are presented for future testing protocol to reduce errors.

1) While setting up camera locations, ensure that the fire source is located within the FOV to ensure a consistent baseline for a comparative activation time.
2) Make sure that all cameras are set at the same viewing angle and aligned horizontally with a laser so that the cameras FOV can be determined.
3) Minimize air currents around the fire source with the intent to obtain accurate results, i.e., optical density and temperature measurements.
4) Method to heat smoke emitters should provide a constant heat output

Additionally, due to a lack of comprehensive variables tested within this research, an outline of important parameters are listed to ensure a better understanding of the effect of each variable.

1) Different smoke colors should be tested with a range of background colors to better understand the effect of a contrast ratio threshold.
2) Range of heating sources to provide more thermal buoyancy to smoke.
3) Repetitive tests to compensate for anomalies in individual tests.
4) Test the system for smaller height enclosures and varying distances from the fire source to better understand the effect of volume of space and distance on activation.

Furthermore, the focus to try and correlate a relationship for the optical density of the plume instead of a plume outline growth rate and contrast ratio dependence would be

advantageous. This would give a fire protection engineer the ability to use the correlation for a performance based design from understood parameters, i.e., HRR and fuel type.

References

[1] Rose-Pehrsson, S.L., Owrutsky, J.C., Gottuk, D.T., Geiman, J.A., Williams, F.W., Farley, J.P., "Phase I: FY01 investigative study for the advanced volume sensor," NRL/MR/6110-03-8688, US Naval Research Laboratory, <http://stinet.dtic.mil>; June 30, 2003.

[2] axonX, "FSM-8 Smoke & Fire Detection System Operation Manual," Sparks, MD, September 2006.

[3] Fastcom Technology., Boulevard de Grancy 19A, 1006 Lausanne, Switzerland, <http://www.fastcom.ch>, June 7, 2007.

[4] Fire Sentry Corporation., 593 Apollo Street, Brea, CA 92821, <http://www.firesentry.com>, June 7, 2007.

[5] Rose-Pehrsson, S.L., Minor, C.P., Steinhurst, D.A., Owrutsky, J.C., Lynch, J. A., Gottuk, D.T., Wales, S.C., Farley, J.P., Williams, F.W., "Volume sensor for damage assessment and situational awareness," *Fire Safety Journal*, Vol. 41, pp. 301-310, 2006.

[6] Gottuk, D.T., Harrison, M.A., Scheffey, J.L., Rose-Pehrsson, S.L., Williams, F.W., Farley, J.P., "An initial evaluation of video-based fire detection technologies," NRL/MR/6180-04-8737, US Naval Research Laboratory, <http://stinet.dtic.mil>; January 9, 2004.

[7] Wright, M.T., Gottuk, D.T., Darwin, R.T., Back, G.G., Peters, A., Farley, J.P. and Williams, F.W., "CVNX Fire Threat to Ordnance: Revised Test Plan for Test Series 2 - Magazine Detection System Response," NRL Letter Report 6180/0159, April 7, 2003.

[8] Gottuk, D.T., Harrison, J.C., Rose-Pehrsson, S.L., Owrutsky, J.C., Williams, F.W., and Farley, J.P., "Video Image Detection (VID) Systems and Fire Detection Technologies: Preliminary Results from the Magazine Detection System Response Tests, " NRL Ltr Rpt 6180/0262, July 21, 2003.

[9] Gottuk, D.T., Harrison, J.C., Rose-Pehrsson, S.L., Owrutsky, J.C., Williams, F.W., and Farley, J.P., "Shipboard Evaluation of Fire Detection Technologies for Volume Sensor Development: Preliminary Results, " NRL Ltr Rpt 6180/0282, August 28, 2003.

[10] Lynch, J.A., Gottuk, D.T., Rose-Pehrsson, S.L., Owrutsky, J.C., Steinhurst, D.A., Minor, C.P., et al. "Volume Sensor development test series 2 – lighting conditions, camera settings, and spectral and acoustic signatures," NRL/MR-MM/6180-04-88843, US Naval Research Laboratory, <http://stinet.dtic.mil>; November 11, 2004.

[11] Lynch, J.A., Gottuk, D.T., Rose-Pehrsson, S.L., Owrutsky, J.C., Steinhurst, D.A., Minor, C.P., Wales, S.C., Williams, F.W., and Farley, J.P., "Test Report Volume Sensor Development Test Series 3 Results - Multi-Component Prototype Evaluation," NRL Ltr Rpt 6180/0353, Naval Research Laboratory, Washington, DC, September 20, 2004.

[12] Lynch, J.A., Gottuk, D.T., Owrutsky, J.C., Steinhurst, D.A., Minor, C.P., Wales, S.C., Rose-Pehrsson, S.L., Farley, J.P., and Williams, F.W., "Volume Sensor Development Test Series 4 Results – Multi-Component Prototype Evaluation," NRL/MR/6180-06-8934, US Naval Research Laboratory, <http://stinet.dtic.mil>; January 25, 2006.

[13] Lynch, J.A., Gottuk, D.T., Owrutsky, J.C., Steinhurst, D.A., Minor, C.P., Wales, S.C., Farley, J.P., Rose-Pehrsson, S.L., and Williams, F.W., "Volume Sensor Development Test Series 5 – Multi-Compartment System" NRL/MR/6180-05-8931, US Naval Research Laboratory, <http://stinet.dtic.mil>; December 30, 2005.

[14] Kouchinsky, A.J., and Milke, J.A., "Analysis of Response Characteristics of CCTV Surveillance for Fire Detection," Department of Fire Protection Engineering, University of Maryland, July 2007.

[15] Glockling, J. and Edwards, M., "Shipboard Intelligent Fire Suppression Systems," White Paper, <www.axonX.com>, 2007.

[16] Lynch, J.A., private communication with axonX, June 7, 2007.

[17] Heskestad. G., "Fire Plumes, Flame Height, and Air Entrainment" *SFPE Handbook of Fire Protection Engineering,* 3rd ed., National Fire Protection Association, Quincy, MA, 2002.

[18] Heskestad. G., "Fire Plumes" *SFPE Handbook of Fire Protection Engineering,* 2nd ed., National Fire Protection Association, Quincy, MA, 1995.

[19] Mowrer. F.W., "Lag Times Associated with Fire Detection and Suppresion," *Fire Technology,* 26, 3, pp. 244-265 (1990).

[20] Klote, J.H., and Milke, J.A., "Smoke and Tenability," *Principles of Smoke Management*, 2002.

[21] Milke, J.A., Mowrer, F.W., and Torero, J.L., "Investigation Of The Application Of Duct Smoke Detectors In Heating, Ventilating And Air Conditioning Systems," Department of Fire Protection Engineering, University of Maryland, April 5, 2002.

[22] UL 268, "Smoke Detectors for Fire Alarm Signaling Systems," Northbrook: UL, Fifth Edition, September 8, 2006.

[23] Regin HVAC Products, Inc.., 315 Riggs Street, Unit 1, Oxford, CT 06478, <http://www.regin.com>, June 13, 2007.

[24] National Fire Protection Association, NFPA 101 - *Life Safety Code*, Quincy, MA, 2003 edition, pp. 263.

[25] Klimek, R.B., and Wright, T.W., Spotlight-8, version 2005.11.23, [Online]. Available: http://microgravity.grc.nasa.gov/spotlight/

[26] Pyzdek, Thomas, *The Six Sigma Handbook*, McGraw-Hill, 2003.